Formation of mixed paragenesis diamonds during multistage growth – constraints from *in situ* $\delta^{13}C$–$\delta^{15}N$–[N] analyses of Koidu diamonds

Mei Yan Lai [a,*] (meiyan1@ualberta.ca),

Thomas Stachel [a] (tstachel@ualberta.ca),

Richard A. Stern [a] (rstern@ualberta.ca),

Matthew F. Hardman [b] (mhardman@gia.edu),

D. Graham Pearson [a] (gdpearso@ualberta.ca),

Jeff W. Harris [c] (jeff.harris@glasgow.ac.uk)

[a] Department of Earth and Atmospheric Sciences, University of Alberta, Edmonton, Canada

[b] Gemological Institute of America, 5355 Armada Drive, Carlsbad, USA

[c] School of Geographical and Earth Sciences, University of Glasgow, Glasgow, United Kingdom

* Corresponding author

Abstract

Inclusion-bearing diamonds from the Koidu kimberlite complex, Sierra Leone (West African Craton) were analyzed *in situ* for carbon and nitrogen isotope compositions, nitrogen concentrations and nitrogen aggregation states. In a suite of 105 diamonds, 78% contain eclogitic mineral inclusions, 17% contain peridotitic mineral inclusions, and 5% - an unusually high proportion - contain co-occurring eclogitic and peridotitic mineral inclusions indicating a mixed paragenesis. Major and trace element compositions of mineral inclusions from two mixed paragenesis diamonds (one with omphacite + Mg-chromite, the other with eclogitic garnet + forsteritic olivine) were determined. The presence of positive Eu anomalies in centrally located omphacite and eclogitic garnet inclusions indicates derivation from subducted protoliths, formed as igneous cumulates in lower oceanic crust. Mg-chromite (Cr# 85.5; Mg# 65.2) and olivine (Mg# 94.5) inclusions, located in outer portions of the mixed paragenesis diamonds, have compositions indicative of derivation from strongly depleted cratonic peridotites. Given that the olivine Mg# of 94.5 is the highest reported to date for the West African Craton, the eclogitic and peridotitic inclusions in these mixed paragenesis diamonds cannot have precipitated during infiltration of peridotitic substrates by eclogite-derived fluids, as the consequent fluid-rock interaction should lead to Mg# lower than that for the original peridotitic diamond substrate. The different origins of eclogitic and peridotitic inclusions could be explained by physical transport of their host diamonds from eclogitic into peridotitic substrates, possibly along high-strain shear zones, before renewed diamond growth.

Based on the $\delta^{13}C$–$\delta^{15}N$ systematics of the entire inclusion-bearing diamond suite from Koidu, three major compositional clusters are identified. Cluster 1 (eclogitic diamond cores; $\delta^{13}C$ = -33.2 to -14.4 ‰ and $\delta^{15}N$ = -5.3 to +10.1 ‰) bears the isotopic signature of recycled crustal

material (± a mantle component). Cluster 2 (peridotitic diamonds and including the core of a diamond containing omphacite + Mg-chromite; $\delta^{13}C$ = -6.0 to -1.1 ‰ and $\delta^{15}N$ = -4.2 to +9.7 ‰) likely involves mixing of carbon and nitrogen from subducted and mantle sources. Cluster 3 (rims of eclogitic diamonds and including the eclogitic garnet + olivine included diamond and the rim of the omphacite + Mg-chromite included diamond; $\delta^{13}C$ = -7.8 to -3.6 ‰ and $\delta^{15}N$ = -7.9 to -2.1 ‰) matches convecting mantle-derived fluids/melts. The distinct isotopic signatures of the three diamond clusters, together with differences in nitrogen aggregation and cathodoluminescence response between diamond cores and rims, suggest episodic diamond growth during multiple fluid/melt pulses.

Keywords: Diamond; carbon isotopes; nitrogen isotopes; mixed paragenesis; West African Craton

1. Introduction

Mineral inclusions encapsulated within diamonds preserve pristine information about the conditions of the mantle at the time of diamond formation, as they cannot re-equilibrate with their surroundings during mantle residence or kimberlite eruption. Based on inclusion mineralogy and composition, a first order division can be drawn between common lithospheric diamonds that form within the thick lithospheric mantle keels underpinning long-term stable continental areas (cratons) and rare superdeep diamonds originating from beneath (> 250 km depth) (Stachel and Harris, 2008). Lithospheric diamonds are divided into peridotitic, eclogitic and websteritic suites, which represent the mantle substrates for their crystallization. Common peridotitic mineral inclusions are Cr-pyrope garnet, Cr-diopside, forsterite, enstatite, Mg-chromite and Ni-rich sulphide. The

eclogitic suite includes, but is not limited to, pyrope-almandine-grossular garnet, omphacite, kyanite, rutile, coesite, corundum and Ni-poor sulphide. The websteritic suite contains minerals that have compositions that are transitional between the peridotitic and eclogitic suites (Meyer, 1987; Taylor and Anand, 2004; Stachel and Harris, 2008).

Any given lithospheric diamond crystal typically hosts mineral inclusions that are derived from a single suite only (Stachel and Harris, 2008). On some occasions, diamond formation occurs in compositionally changing environments caused by the interaction of metasomatic melts with diamond substrates, which may result in eclogitic and websteritic inclusions being trapped in the same diamond at different stages during diamond growth (Aulbach et al., 2002; Davies et al., 2004a). Diamonds containing both peridotitic and eclogitic mineral inclusions (referred to as "mixed paragenesis" hereafter) are rare and have only been documented from a few localities, e.g., West Africa (Prinz et al., 1975), Argyle in Western Australia (Hall and Smith, 1984), Monastery in South Africa (Moore and Gurney, 1986), Sloan in USA (Otter and Gurney, 1986), Shengli 1 and Pipe 50 in China (Wang, 1998) and the Lac de Gras area in Canada (Davies et al., 2004b). Diamonds of mixed paragenesis are thought to document multiple diamond growth events that occurred in different substrates (Wang, 1998) although other origins are possible, such as modification of mineral compositions by melt-rock reaction in the mantle, accompanied by diamond growth (Mikhail et al., 2021).

In this study, we identify five diamonds from the Koidu kimberlite complex in Sierra Leone that contain both eclogitic and peridotitic mineral inclusions – an unusually high number of diamonds relative to the majority of those recovered. We investigate their formation by imaging diamond growth textures, assessing the chemical compositions of the mixed paragenesis mineral inclusions and by comparing the N concentrations, N aggregation states and stable isotope

compositions of these unusual diamonds to single-paragenesis diamonds from the same locality. This is the first study to employ multi-collector secondary ion mass spectrometry (SIMS) to measure variations in $\delta^{13}C$, $\delta^{15}N$ and N concentration in different growth zones of Koidu diamonds (including peridotitic, eclogitic and mixed paragenesis diamonds) at high spatial resolution, enabling detection of changing growth conditions and therefore the dynamic environment of diamond formation.

2. The West African Craton and Sierra Leone diamonds

Inclusion-bearing diamonds for this study were recovered from the Koidu kimberlite complex and an adjacent sedimentary basin, in the Kono District of eastern Sierra Leone, situated on the Archean Man Shield in the southern part of the West African Craton. The Archean rocks in the Man Shield comprise mainly of 3.26–2.85 Ga tonalite-trondhjemite-granodiorite (TTG) gneisses (up to 3.6–3.5 Ga in age), supracrustal belts containing a basalt-komatiite sequence overlain by sediments, and ca. 2.8 Ga granitoids formed in a craton-wide thermal event (Rollinson, 2016). The whole rock Re-Os isochron age of low-MgO eclogite xenoliths from the Koidu kimberlite complex was found to be 3.4 ± 0.8 Ga, indicating their formation during Archean subduction (Barth et al., 2002a). Recent Sr-U-Pb dating of clinopyroxenes from Koidu eclogite xenoliths also suggested at least Proterozoic and possibly Archean ages, with a preferred age of 2.7 Ga (Aulbach et al., 2019a). The Neoproterozoic break-up of Rodinia may have led to intrusion of a kimberlite-like metasomatic agent in the West African lithosphere (Aulbach et al., 2019b). This metasomatic event may have prompted diamond formation at ca. 0.6 Ga, as indicated by Re-Os isochron ages of sulphide inclusions in diamonds from Zimmi, West Africa, with radiogenic and sulphur stable isotope compositions requiring a subduction origin (Smit et al., 2016, 2019a).

The Koidu kimberlite complex is one of a few localities worldwide where eclogites constitute the only type of mantle xenoliths (Tompkins and Haggerty, 1984; Hills and Haggerty, 1989; Fung and Haggerty, 1995). Despite the absence of peridotite xenoliths, indicator minerals (heavy media separates) from the Koidu kimberlites are both peridotitic and eclogitic (Skinner et al., 2004). A recent study of Koidu indicator minerals documented a large proportion of garnets with high Cr and low Ca contents, indicating the presence of strongly depleted harzburgites or dunites in the underlying lithospheric mantle (Harder et al., 2013).

Diamonds containing either eclogitic or peridotitic inclusions have been recovered from Sierra Leone, though only very limited information has been published. Recovered inclusions include olivine, enstatite, Cr-pyrope, chromite (Meyer and Boyd, 1972) and sulphide (Deines and Harris, 1995; Smit et al., 2016). Carbon isotope analyses of Sierra Leone diamonds are also scarce, with only a few chromite- and sulphide-bearing diamonds from Koidu and Zimmi (Deines and Harris, 1995; Smit et al., 2019b, respectively) having been analyzed, and no N isotope compositions reported.

3. Sample description

A total of 111 inclusion-bearing rough diamonds 2–4 mm in size were studied. The total weight of the diamonds is 10.7 carats. All diamonds in the sample suite are colourless except for one pale yellow and one light brown diamond. Their morphology is dominated by octahedra (n = 85), followed by rounded dodecahedra (n = 11), transitional octahedra-dodecahedra (n = 7), irregular shapes (n = 4), macles (n = 2), an aggregate (n = 1) and an intergrowth of two octahedra (n = 1). Descriptions of diamonds are summarized in Table S1.

Resorption features are observed on all diamonds, with negative trigons occurring on all octahedral faces and aligning in parallel rows where plastic deformation lines are present. Other common resorption features include shield-shaped laminae and hexagonal pits on octahedral faces, hillocks, corrosion sculptures and micro-disk patterns on rounded dodecahedral faces, terraces around the three-fold axes of dodecahedral crystals, and tetragons on presumed {100} faces of irregular-shaped diamonds. Surface textures not restricted to specific crystal faces include deformation lines, ruts, fractures, and a green irradiation spot on an octahedral diamond. Voids of cubo-octahedral shapes are found on the surface of some diamonds, likely representing cavities previously occupied by mineral inclusions. Examples of common surface textures of Koidu diamonds can be found in Fig. S1.

Six diamonds contained only crustal mineral inclusions (epigenetic) and thus they were not further investigated. From 105 diamonds, 370 primary mineral inclusions were recovered, and we found that 82 diamonds (78%) contained eclogitic inclusions, 18 diamonds (17%) contained peridotitic inclusions, and five diamonds (5%) contained both eclogitic and peridotitic inclusions. The chemical composition of mineral inclusions in single-paragenesis Koidu diamonds will not be discussed further in the current manuscript.

The five diamonds of mixed paragenesis are 130-9 (omphacite + olivine), 130-31 (coesite + olivine), 133-6 (omphacite + Mg-chromite), 138-7 (eclogitic garnet + olivine) and 146-1 (olivine + Mg-chromite + coesite). Omphacite, olivine and coesite inclusions are all colourless, but were identified using their chemical compositions. The spatial distribution of particular inclusions within their host diamonds and consequently the direction of changes in inclusion composition could only be investigated for two diamonds containing mineral inclusions with clearly distinguishable colours — diamonds 133-6 and 138-7. The chemical composition of the mineral

inclusions in these two diamonds are discussed in detail below, whereas the inclusion compositions of the other mixed paragenesis diamonds are reported in Table S3. In both diamonds, eclogitic inclusions are located in the centre and peridotitic inclusions near the rim (Fig. 1).

4. Analytical methods

4.1 Mineral inclusions

Mineral inclusions were mounted with epoxy resin in 6 mm diameter brass tubes and polished. Initial mineral identification was achieved by back-scattered electron (BSE) imaging and energy dispersive spectroscopy (EDS). Major and minor element compositions were determined using CAMECA SX100 and JEOL JXA-8900R electron probe microanalyzers (EPMA), both equipped with five wavelength-dispersive spectrometers (WDS). The instruments were operated at an accelerating voltage of 20 kV, a beam current of 20 nA, and a fully-focussed beam with a diameter < 1 μm. Reference materials include metals and natural and synthetic minerals. For all elements, the Kα emission lines were employed for analysis. The counting time was 20–100 s on the peak, with resulting oxide detection limits typically ≤ 0.02 wt%. Three spots were measured on each grain and, after assessing compositional homogeneity, the compositions of the spots were averaged.

Trace elements (including REE, Ti, V, Ni, Rb, Sr, Zr, Nb, Ba and Hf) in garnet and clinopyroxene inclusions were determined using a Resonetics M-50-LR 193 nm ArF excimer laser ablation system, with a Laurin-Technic S-155 two-volume ablation cell, coupled with a Thermo Scientific Element IIXR inductively coupled plasma mass spectrometer (LA-ICP-MS). Mineral inclusions were ablated with a spot size of 23–90 μm at a frequency of 10 Hz and a laser fluence

of ~4 J/cm^2. Analysis of each sample includes 40 s background collection followed by 60 s sample ablation/measurement and 40 s washout. Detection limits are typically ≤ 40 ppb for REE, V, Rb, Sr, Zr, Nb, Ba and Hf, and ≤ 1 ppm for Ti and Ni. Calibration was achieved using the NIST SRM 612 glass standard and ^{43}Ca as internal standard for data processing. USGS reference glass BIR-1G was analysed as an unknown and the results were compared to the GeoRem preferred values (Jochum et al., 2005) to assess repeatability and accuracy.

4.2 Host diamonds

Infrared absorption spectra of diamonds were obtained before crushing, using a Thermo Fisher Nexus 470 Fourier transform infrared (FTIR) spectrometer equipped with a Continuum IR microscope. An aperture size of 100 × 100 μm was used in transmission mode. Spectra were acquired by averaging 200 scans at a spectral resolution of 1 cm^{-1} with a spectral range of 4000–650 cm^{-1}. Baseline-corrected spectra were normalized to 1 cm diamond thickness, where the absorption coefficient for the intrinsic absorption of diamond at 1995 cm^{-1} is approximately 11.94 cm^{-1} (e.g., Howell et al., 2012). Nitrogen concentrations and aggregation states of diamonds were calculated by deconvolution of the normalized spectra, where [N_A] = 16.5 × μA (absorption coefficient at 1282 cm^{-1} for the A-centre; Boyd et al., 1994a) and [N_B] = 79.4 × μB (absorption coefficient at 1282 cm^{-1} for the B-centre; Boyd et al., 1995). The detection limit for N is ~5 at.ppm. More than one spectrum was collected for diamonds at different spots. Note that the N distribution in diamond may be heterogeneous, and the infrared absorption spectrum is an integrated signal collected over the optical path of the diamond, which may contain different growth zones with distinctly different N contents.

Diamond fragments were first cast in epoxy and then ground and polished. Subsequently, the fragments were co-mounted in indium with a SIMS reference material – diamond S0270. Prior

to analysis, cathodoluminescence (CL) images of diamond fragments were obtained using a Zeiss EVO MA15 scanning electron microscope (SEM) equipped with a parabolic mirror coupled to a high sensitivity broadband photomultiplier tube to reveal the diamond internal growth textures. The mount was coated with Au to prevent charging during SEM operation. The scanning electron microscope was operated at a voltage of 15 kV and a beam current of 3–5 nA. Subsequently, C and N isotope compositions and N abundances of the mounted diamond fragments were determined using a CAMECA IMS-1280 multi-collector ion microprobe. Two to eight measurement spots were set on each diamond fragment to cover all growth zones. The primary beam of 20 keV $^{133}Cs^{+}$ ions was focused to a beam diameter of approximately 10 μm, with beam currents of 2 nA, 2.5–3.0 nA and 0.6 nA for the analyses of C isotope composition, N isotope composition and N abundance, respectively. Carbon isotopes were analyzed first, followed by N abundance and N isotope measurements from the same spot location. The detection limit for N abundance is ~0.1 at.ppm. Nitrogen isotope compositions were only measured on spots with N abundance > 65 at.ppm. Carbon isotope compositions are reported as $\delta^{13}C_{VPDB}$, which is the normalized difference of the $^{13}C/^{12}C$ ratio of the sample relative to that of the Vienna Pee Dee Belemnite standard ($^{13}C/^{12}C_{VPDB}$ = 0.01118; Coplen et al., 2002). Nitrogen isotope compositions are reported as $\delta^{15}N_{AIR}$, which is the normalized difference of the $^{15}N/^{14}N$ ratio of the sample relative to that of the atmosphere ($^{15}N/^{14}N_{AIR}$ = 0.003677; Junk and Svec, 1958). The analytical sequences for C and N isotopes interspersed measurements of unknowns with diamond reference S0270 ($\delta^{13}C_{VPDB}$ = -8.88 ± 0.10 ‰; $\delta^{15}N_{AIR}$ = -0.40 ± 0.50 ‰; Stern et al., 2014) in a 4:1 ratio. Uncertainties of individual $\delta^{13}C_{VPDB}$ analyses for diamond S0270 and unknowns are typically ±0.14 ‰ (2σ). Uncertainties of individual $\delta^{15}N_{AIR}$ analyses are typically ±0.60 ‰ (2σ) for diamond S0270, and typically range from ±0.50 to ±4.0 ‰ (2σ) for unknowns with N concentration ranging

223 from 2500 to 50 at.ppm, respectively. Additional details of the analytical procedure were outlined
224 in Stern et al. (2014).

225

226 **5. Results**

227 **5.1 Mineral inclusions from mixed paragenesis diamonds**

228 **5.1.1 Diamond 133-6**

229 Diamond 133-6 contains four omphacites (clinopyroxenes with a jadeite component ≥ 20
230 and < 80 mol%; Clark and Papike, 1968) within a radius of ~500 μm in the centre and one Mg-
231 chromite in the rim (Fig. 1a). The omphacites were surrounded by small fractures, which did not
232 extend to the surface of the diamond. Backscattered electron images indicated that all inclusions
233 have homogeneous compositions throughout the grains. Inter-grain variation among the four
234 omphacites was negligible, thus an average major element composition is reported.

235 The omphacites have high molar Mg# (100×Mg/[Mg+Fe] = 82.2) and jadeite component
236 (100×2Na/[2Na+Ca+Mg+Fe] = 63.9 mol%). The Ca-Mg-Fe compositions of these omphacites are
237 similar to the omphacites from Koidu gabbroic eclogites (classified based on bulk-rock $[Eu/Eu^*]_N$
238 ≥ 1.05, where $Eu^* = [Sm_N \times Gd_N]^{0.5}$; Aulbach et al., 2019b) and low-MgO eclogites (bulk-rock
239 MgO content = 6–13 wt%; Hills and Haggerty, 1989; Aulbach et al., 2019b) (Fig. 2). The average
240 Cr_2O_3 content in these omphacites is very low (≤ 0.02 wt%) (Table 1).

241 Trace element compositions were determined for three of the omphacites from diamond
242 133-6 (Table 2). They have very similar REE_N patterns and show positive Eu anomalies (defined
243 as $[Eu/Eu^*]_N > 1$), with $[Eu/Eu^*]_N$ = 1.63–1.78. The REE_N patterns of these omphacites are clearly

different from omphacites in Koidu eclogite xenoliths (Aulbach et al., 2019b) (Fig. 3). The omphacite inclusions are enriched in LREE relative to CI-chondrite, but have unusually low MREE and HREE compared to clinopyroxene inclusions in diamonds worldwide (Stachel and Harris, 2008), resulting in high LREE/HREE ratios. The concentrations of the HREE Tm, Yb and Lu are below the limit of detection, except for Yb in one omphacite. They also are enriched in Nb, Sr, Ti and V relative to CI-chondrite (Fig. 4).

The Mg-chromite inclusion has a cubo-octahedral morphology and no associated fractures, implying a synchronous relationship with the growth zone of the host diamond in which it occurs. It has high Mg# (65.2) and Cr# (100×Cr/[Cr+Al] = 85.5), typical for peridotitic spinel inclusions in diamond worldwide (Stachel and Harris, 2008).

5.1.2 Diamond 138-7

Diamond 138-7 contains five eclogitic garnets in the centre and one olivine in the rim (Fig. 1b). No fractures are observed around the inclusions nor elsewhere in this diamond. All inclusions grains are internally compositionally homogeneous, without any sign of alteration.

Garnets show significant grain to grain compositional variations in SiO_2 (39.5–41.9 wt%), Al_2O_3 (21.9–23.9 wt%), MgO (8.1–9.7 wt%) and CaO (16.7–19.3 wt%) (Table 1). The very high CaO contents are unusual and worldwide, garnet inclusions with CaO contents $\geq$ 17 wt% have been reported only from a few localities, most prominently Klipspringer in South Africa (Westerlund and Gurney, 2004), the New South Wales alluvials (Davies et al., 2003) and Argyle in Australia (Jaques et al., 1989), but have not been observed at other localities on the West African Craton. Among Koidu eclogite xenoliths, similar high CaO in garnet is only seen in a few low-MgO kyanite or corundum eclogites (Hills and Haggerty, 1989) (Fig. 5).

Trace element compositions of three garnets from diamond 138-7 were determined (Table 2). Their REE_N patterns are very similar to one another, with small differences in La and from Eu to Lu (Fig. 6). All garnets have positive Eu anomalies, with $[Eu/Eu^*]_N$ = 1.10–1.41. They have REE_N patterns typical of cratonic eclogite xenoliths, characterised by increasing abundances from subchondritic La to about 10x chondritic MREE and HREE (Sm to Lu). Their MREE to HREE contents overlap with the field of garnets from Koidu gabbroic eclogites (Aulbach et al., 2019b), with the LREE La to Pr above the xenolith garnet range. Strontium and Nb abundances are subchondritic (Fig. 7). There are positive correlations between trace element and major element compositions, where Nb and Ti increase with CaO abundance in these garnets (Tables 1 and 2).

The single olivine inclusion is elongated in shape. It has a very high Mg# (94.5), documenting the strongly depleted nature of the harzburgitic to dunitic diamond substrates. On the West African Craton, such high Mg# have only been reported for retrograde olivines occurring as inclusions in sublithospheric diamonds (Kankan, Guinea; after primary wadsleyite or ringwoodite; Stachel et al., 2000a), but not for olivine in lithospheric diamonds (Meyer and Boyd, 1972 ; Stachel and Harris, 1997; Stachel et al., 2000b).

5.2 $\delta^{13}C$, $\delta^{15}N$ and N concentrations in Koidu diamonds

5.2.1 Peridotitic diamonds

Peridotitic diamonds from Koidu (18 diamonds; 54 SIMS analyses; Tables 3 and S3) have a restricted range in $\delta^{13}C$ values from -6.0 to -1.1 ‰, well within the range of peridotitic diamond worldwide (Stachel et al., 2009) (Fig. 8a). Their N abundances (all values stated in section 5.2 were obtained by SIMS) and $\delta^{15}N$ values range from 0.4 to 920 at.ppm (median = 80 at.ppm) and -4.2 to +9.7 ‰, respectively, and define one of three clusters (Cluster 2) shown in Fig. 9 (see

Section 6.4 for detailed discussion). Three peridotitic diamonds have mantle-like isotopic signatures (defined as $\delta^{13}C = -5 \pm 3$ ‰ and $\delta^{15}N = -5 \pm 3$ ‰; Cartigny et al., 2014) with $\delta^{13}C$ values of -5.7 to -2.6 ‰ and $\delta^{15}N$ values of -4.2 to -2.1 ‰ (Fig. 9), accompanied by variable N contents (1–680 at.ppm). Most diamonds have small internal variations in C isotope composition (average $\sigma < 0.2$ ‰), except for four diamonds (130-21, 130-25, 134-2 and 136-1; Table S4) which have intra-diamond $\delta^{13}C$ variations up to 2.8 ‰.

5.2.2 Eclogitic diamonds

Koidu eclogitic diamonds in this study (82 diamonds, 321 SIMS analyses; Tables 3 and S3) show highly variable isotope compositions and N concentrations, indicating growth during multiple events. Based on their $\delta^{13}C$ and $\delta^{15}N$ values, they define two additional clusters (Clusters 1 and 3; Fig. 9), which will be discussed in Section 6.4 in detail.

Based solely on their $\delta^{13}C$ values, the eclogitic diamonds can be separated into three subgroups:

^{13}C-enriched diamond: This group contains only a single diamond with the highest $\delta^{13}C$ values among Koidu eclogitic diamonds. The bulk of this diamond has $\delta^{13}C$ values from -1.8 to 0.0 ‰ and negligible N content. Lower $\delta^{13}C$ values (-4.2 ‰) are observed in a more N-rich (50–80 at.ppm) growth zone. $\delta^{15}N$ values were not determined for this overall N-poor diamond.

^{13}C-depleted diamond: Diamonds in this group have $\delta^{13}C$ values from -33.2 to -15.1 ‰, with ~80% of the data falling in the range of -30 to -25 ‰ (Fig. 8b). Compared to Koidu peridotitic diamonds, this group has a broader range of N abundances (0.4 to 2080 at.ppm; median = 30 at.ppm) and $\delta^{15}N$ values (-5.3 to +9.9 ‰; Fig. 9). Most diamonds are internally homogeneous in carbon isotope composition, but with a spread in $\delta^{15}N$ values of up to 5.4 ‰. Six diamonds in this

group have a less ^{13}C-depleted outermost growth zone ($\delta^{13}C$ = -19.2 to -15.1 ‰) compared to the core ($\delta^{13}C$ = -29.6 to -24.9 ‰).

Diamonds with cores depleted in ^{13}C and rims with mantle-like C isotopic signature: Twenty-four diamonds have a clear core-rim structure (core and rim have distinctly different CL brightness), where the core zone has low $\delta^{13}C$ values (-30.2 to -14.4 ‰) and generally low N concentrations (1–890 at.ppm; median = 30 at.ppm), while the rim has higher, mantle-like $\delta^{13}C$ values (-7.8 to -5.6 ‰) and high N concentrations (610–2200 at.ppm; median = 870 at.ppm) (Figs. 8c and 10). For the core zones, only 12 diamonds have sufficiently high N abundances (> 65 at.ppm) to allow for precise N isotope analysis; $\delta^{15}N$ values in the cores range from -5.6 to +8.1 ‰, overlapping with the range for the subgroup of ^{13}C-depleted eclogitic diamonds (see above). The high N abundances in the rims allow the measurement of N isotope compositions for all diamonds in this group, indicating mantle-like $\delta^{15}N$ values between -7.9 and -2.6 ‰ (Fig. 9). One diamond in this group has a distinct intermediate layer between the core and the rim, with an average $\delta^{13}C$ value of -15.3 ‰ that is ~10 ‰ higher than the core zone and ~8 ‰ lower than the rim, but similar to the outermost growth zones of the six zoned ^{13}C-depleted eclogitic diamonds (see above). $\delta^{15}N$ values of this diamond fluctuate from -0.5 ‰ in the core zone to +10.1 ‰ in the intermediate layer to -5.5 ‰ in the rim.

5.2.3 Mixed paragenesis diamonds

The isotope compositions of all studied mixed paragenesis diamonds (5 diamonds, 89 SIMS analyses) are shown in Figs. 8d and 9, and together with N concentrations listed in Tables 3 and S3. These mixed paragenesis diamonds lie within the three clusters (Fig. 9) mentioned above and will be discussed in detail in Section 6.4.

Diamond 133-6 (omphacite and Mg-chromite included) is comprised of inner growth zones and a rim with similar $\delta^{13}C$ (-4.8 to -3.6 ‰) but distinct $\delta^{15}N$ values and N contents. The inner growth zones have a broad range of N isotope compositions ($\delta^{15}N$ = -6.2 to +4.8 ‰) and low N contents (1–380 at.ppm). The rim has a restricted, mantle-like N isotopic signature ($\delta^{15}N$ = -7.9 to -6.7 ‰) and high N contents (520–750 at.ppm). Core-to-rim transects show that within the innermost zone of this diamond (fragments 1 and 3 in Fig. 11) a minor outward increase in $\delta^{13}C$ values (from -4.7 to -3.7 ‰) is accompanied by decreasing N concentrations (from 330 to 20 at.ppm), but no trend in $\delta^{13}C$ values is observed for the intermediate or rim zones.

Diamond 138-7 (eclogitic garnet and olivine included) does not have a discernible core-rim zonation. Carbon and N isotope compositions vary ($\delta^{13}C$ = -5.3 to -4.1 ‰; $\delta^{15}N$ = -9.8 to -5.3 ‰) within the mantle range. Nitrogen abundance varies widely, from 1 to 1050 at.ppm. Although multiple growth zones and some mild resorption at the outer boundary of the inner growth zone are observed, the zones generally have a homogeneous CL response and transects across them do not reveal coherent trends in $\delta^{13}C$ values.

Diamonds 130-31 (coesite and olivine included) and 146-1 (coesite, Mg-chromite and olivine included) have isotope compositions ($\delta^{13}C$ = -4.7 to -1.3 ‰; $\delta^{15}N$ = -2.3 to +5.8 ‰) and N contents (0.3–340 at.ppm) within the range of peridotitic Koidu diamonds. Diamond 130-9 (omphacite and olivine included) has an isotopic signature ($\delta^{13}C$ = -24.8 to -22.6 ‰; $\delta^{15}N$ = -4.1 ‰) and N contents (0.9–180 at.ppm) similar to the ^{13}C-depleted eclogitic diamonds in this study.

5.3 Nitrogen aggregation in episodically grown diamonds

Nitrogen is incorporated into the diamond lattice in the form of single substitutional N (C-centres; Taylor et al., 1996; Type Ib) during crystallization. Residence in the mantle at high

temperature leads to the diffusion and combination of single N atoms into pairs (A-centres; Davies, 1976; Type IaA). Nitrogen pairs further aggregate to a structure of four N atoms surrounding a vacancy (B-centre; Jones et al., 1992; Type IaB), along with the generation of two side products – the N3 centre (three N atoms surrounding a vacancy) and platelets (aggregations of interstitial C atoms) (Woods, 1986). The rate of N aggregation depends on three major factors – mantle residence temperature, mantle residence time and N concentration in diamonds (e.g., Taylor et al., 1990).

Cathodoluminescence images of the episodically grown diamonds show a relative relationship of bright cores and dark rims (Fig. 10), indicating low concentrations of optically active lattice defects to cause CL in the rims. Infrared absorption spectra (Table S1, S2 and Fig. 12) show that the brighter cores contain N in higher aggregation states (Type IaAB with $\geq$ 30 %B), where N3 centres (with a luminescent wavelength at 415 nm; Zaitsev, 2001) are present, while the rims represent overgrowths of diamond with lower N aggregation states dominated by A-centres, which are known to quench luminescence (Vasil'ev et al., 2004). Enhanced N aggregation states in the cores indicate that they had longer mantle residence times or higher mantle storage temperatures compared to the rims (Taylor et al., 1990; Leahy and Taylor, 1997), documenting that cores and rims in these diamonds formed during distinct growth events separated in time or in temperature.

6. Discussion

6.1 Origin of eclogitic mineral inclusions in Koidu mixed paragenesis diamonds

Positive Eu anomalies in omphacites from diamond 133-6 and garnets from diamond 138-7 indicate accumulation of plagioclase in their protoliths (Schmickler et al., 2004), suggesting a protolith origin as gabbro cumulates. Major element compositions of both omphacite and garnet inclusions are similar to some Koidu kyanite- and corundum-bearing low-MgO eclogite xenoliths (Hills and Haggerty 1989), and trace element compositions (MREE to HREE) of garnet inclusions are similar to garnet from Koidu gabbroic eclogite xenoliths (Aulbach et al., 2019b), suggesting that the eclogitic inclusions in mixed paragenesis diamonds inherited compositional characteristics of their eclogitic diamond substrates.

Omphacites from diamond 133-6 have highly fractionated REE_N patterns ($La_N/Yb_N = 422$) that are very different from typical eclogitic clinopyroxenes, which usually have humped patterns with $La_N/Nd_N < 1$ and higher HREE contents (e.g., Jacob, 2004). Omphacites with overall very similar REE_N and $HFSE_N$ patterns at lower LREE (Figs. 3 and 4) were, however, observed in two low-MgO eclogites from Obnazhennaya in Siberia (Sun et al., 2020) and a kyanite eclogite from Bellsbank in South Africa (Shu et al., 2016). This similarity in trace element patterns does not fully extend to major element compositions, where the omphacites from diamond 133-6 and from Obnazhennaya and Bellsbank are distinct in their Mg# (82.2 versus 88.8 and 88.4, respectively) and jadeite content (63.9 versus 22.1 and 46.5 mol%, respectively). The protoliths of Obnazhennaya low-MgO and Bellsbank kyanite eclogites were suggested to be olivine gabbro cumulates (Shu et al., 2016; Sun et al., 2020). Eclogites with cumulate protoliths are inferred to have incorporated a trapped melt component and subsequently, during subduction, to have experienced eclogite-facies melt extraction (Aulbach et al., 2007; Aulbach and Jacob, 2016; Sun et al., 2020). Without coexisting garnet, we cannot evaluate the origin of the clinopyroxene inclusions in diamond 133-6 in detail, but based on their high similarity in trace element

composition to the Obnazhennaya and Bellsbank clinopyroxenes we suggest a similar origin, i.e., that the clinopyroxene inclusions derived from oceanic cumulates (possibly with trapped melt) that were subducted and metamorphosed. In addition, the diamond substrate could have been affected by a subsequent stage of metasomatic LREE enrichment to explain the significantly higher contents in La to Pr relative to Obnazhennaya and Bellsbank clinopyroxenes (Fig. 3).

The high and variable CaO contents in the garnets from diamond 138-7 may reflect continued metasomatic enrichment during diamond growth. This was previously suggested for an eclogitic diamond from the Mir kimberlite containing 35 garnet inclusions with a wide range of CaO contents (Sobolev et al., 1998). Multiple olivine inclusions with different CaO contents in a single Kankan diamond were also attributed to metasomatic Ca enrichment during diamond growth (Stachel et al., 2000b). The observed positive correlations of Ca with Nb and Ti for the garnets from diamond 138-7 indicate that the metasomatic process accompanying diamond formation could have affected trace elements. Elevated LREE in the garnet inclusions relative to garnets from Koidu gabbroic eclogite xenoliths (Aulbach et al., 2019b) appear to support this interpretation. A possible metasomatic agent driving diamond precipitation and enrichment in Ca and LREE could be a low-Mg carbonatitic high-density fluid or a carbonatitic melt (Sobolev et al., 1998; Stachel et al., 2000b; Klein-BenDavid et al., 2009). Alternatively, the difference in LREE concentrations between inclusion and gabbroic eclogite xenolith garnets may be attributed to crystal-chemical effects: the Ca# (Ca/[Ca+Mg+Fe+Mn]) of garnet strongly influences partitioning of trace elements between garnet and pyroxene, with both the REE concentrations and the LREE/HREE ratio in garnet increasing together with $Ca\#_{garnet}$ (Harte and Kirkley 1997; Aulbach et al., 2017).

Either way, two key observations suggest that the garnet inclusions in diamond 138-7 predominantly reflect their substrate composition: (1) the presence of positive Eu anomalies and (2) the overall shape of the REE_N patterns, which are typical for garnets in eclogites with low-pressure protoliths that experienced some cumulate enrichment (lowering the REE overall) and possibly partial melting during or after subduction (preferentially extracting LREE) (Ireland et al., 1994; Barth et al., 2001; Stachel et al., 2004; Aulbach and Jacob, 2016).

6.2 Progressive precipitation of eclogitic and then peridotitic inclusions from an evolving eclogite-derived fluid

Geochemical modelling, based on the Extended Deep Earth Water (DEW) model, indicated that the interaction between eclogite-derived fluids and a range of mantle peridotite compositions may result in the progressive formation of eclogitic, websteritic and peridotitic minerals (Mikhail et al., 2021). If captured in the form of inclusions during associated diamond growth, this model predicts the occurrence of inclusions of different paragenesis in single diamonds. The calculated models predict 2-3 vol% spinel in the final mineralogy resulting from fluid-peridotite interactions, which seemingly appears to fit with our observation of spinel (chromite) in mixed paragenesis diamond 133-6. With the caveat that the minor element Cr is not included in the DEW model runs, the predicted spinel-group mineral, however, is magnetite, which is a very rare inclusion in diamond (Stachel et al., 1998). Instead, the spinel inclusion found in the rim of diamond 133-6 is a Mg-chromite, with the high Mg# (65.2) and Cr# (85.5) typical of garnet-facies spinels found in cratonic peridotite xenoliths and as inclusions in diamonds (McDonough and Rudnick, 1998; Stachel and Harris 2008). Similarly, the olivine inclusion near the rim of mixed paragenesis diamond 138-7 bears the highly magnesian character (Mg# 94.5) of strongly depleted cratonic peridotites, very much unlike the expected product of a process that converts depleted peridotite

into websterite (Mallik and Dasgupta, 2012, 2013). As discussed in the preceding section, the centrally located eclogitic garnet and omphacite inclusions also are very much alike eclogite xenolith minerals and bear the characteristics of subducted gabbroic protoliths rather than those of an eclogite-derived fluid. The very high CaO content of the eclogitic garnet inclusions precludes equilibration with orthopyroxene and consequently, derivation from websterite, which is the product of the modelled fluid-rock interactions (Mikhail et al., 2021). Thus, we conclude that the peridotitic inclusions in our samples are not the result of extended eclogitic fluid-peridotite reactions but instead must have a separate origin from the "coexisting" eclogitic inclusions. Furthermore, with their distinct CL responses and N concentrations, the core and rim zones of diamond 133-6 (Fig. 11) suggest episodic diamond growth rather than fluid evolution during a single metasomatic event.

6.3 Covariation of $\delta^{13}C$ values and N abundance

In the published literature, N is generally considered as a compatible element in diamond, incorporated through equilibrium partitioning with the diamond-forming fluid/melt, with $K_N^{diamond\text{-}fluid} \geq 2$ for diamond crystallization from a reduced medium (Thomassot et al., 2007; Smit et al., 2019b), and $K_N^{diamond\text{-}fluid} \geq 4$ for diamond growth from an oxidized medium (Stachel et al., 2009; Smart et al., 2011; Petts et al., 2015). Therefore, progressive diamond formation from a single pulse of fluid/melt should lead to a gradual decrease in N concentration.

Assuming precipitation from a single C species in the fluid/melt, diamond showing a trend of outward decreasing N concentration accompanied by increasing or decreasing $\delta^{13}C$ values reflects diamond formation from an oxidized (CO_2 or CO_3^{2-}) or a reduced medium (CH_4), respectively (Deines, 1980). Thus, the core-to-rim transects showing progressively decreasing N concentrations and increasing $\delta^{13}C$ values within the innermost growth zone of diamond 133-6

may indicate an oxidized diamond-forming medium (Fig. 11). Alternatively, precipitation from a mixed CHO fluid, containing both CH_4 and CO_2 in variable ratios, would also lead to ^{13}C enrichment during diamond precipitation under fluid-limited conditions (Stachel et al., 2017). The same covariation is not observed in the intermediate zones and the rim of this diamond (Fig. 11), suggesting that they did not form from the same pulse of fluid/melt as the innermost zone. In addition, N abundance within the rim of diamond 133-6 is consistently high and systematic variations in stable isotope composition are absent, implying that the final growth stage did not occur in a fluid/melt-limited system, in contrast with the innermost growth zone showing systematic N and $\delta^{13}C$ variations that point to a fluid/melt-limited system.

Diamond 138-7 has overall high N concentrations, except for minor growth zones that have N < 100 at.ppm. The absence of a systematic covariations in $\delta^{13}C$ and N abundance again suggests diamond formation in a system that was not fluid/melt-limited. Although mild resorption is observed at the outer boundary of the inner growth zone, this diamond has homogeneous CL brightness and shows overall small variations in isotope compositions, suggesting that it either formed from two pulses of a related fluid or during protracted growth from fluids with similar isotope compositions and N contents.

6.4 Sources of C and N in Koidu diamonds

The variation of $\delta^{13}C$–$\delta^{15}N$ in Koidu diamonds indicates the presence of three major clusters (Fig. 9). Cluster 1 is characterised by depletion in ^{13}C and highly variable $\delta^{15}N$ values ($\delta^{13}C$ = -33.2 to -14.4 ‰; $\delta^{15}N$ = -5.3 to +10.1 ‰); it comprises diamonds with eclogitic inclusions and mixed paragenesis diamond 130-9 (Fig. 13a). Cluster 2 shows mantle-like to mildly ^{13}C-enriched C isotope compositions and again a large spread of $\delta^{15}N$ values ($\delta^{13}C$ = -6.0 to -1.1 ‰; $\delta^{15}N$ = -4.2 to +9.7 ‰); it includes mainly peridotitic diamonds and three mixed paragenesis

diamonds – 133-6 (core zone only), 130-31 and 146-1 (Fig. 13a). Cluster 3 has a mantle-like isotopic signature ($\delta^{13}C$ = -7.8 to -3.6 ‰; $\delta^{15}N$ = -7.9 to -2.1 ‰) and includes the rims of eclogitic diamonds and mixed paragenesis diamonds 138-7 and 133-6 (rim only) (Fig. 13b). The assignment of mixed paragenesis diamonds to either Cluster 2 or 3 is entirely based on their N isotope composition, with their $\delta^{13}C$ values remaining approximately constant over the entire $\delta^{15}N$ range from ~ -10 to +10 ‰.

Cluster 1: The ^{13}C-depleted signature of our Koidu eclogitic diamonds is also observed in previously studied sulphide-bearing eclogitic diamonds from Koidu ($\delta^{13}C$ = -33.0 to -16.3 ‰; Deines and Harris, 1995). In a suite of five sulphide-bearing eclogitic diamonds from Zimmi (Sierra Leone), which are alluvial diamonds thought to derive from a subcontinental lithospheric mantle source similar to Koidu, three show similar ^{13}C-depleted signatures ($\delta^{13}C$ = -24.5 to -16.1 ‰) while the remaining two have $\delta^{13}C$ between -8.3 and -6.7 ‰ (Smit et al., 2019b). Since $\delta^{15}N$ was not analysed in these two previous studies, it is not possible to assign these diamonds to the three clusters defined in this study. The much wider range of $\delta^{13}C$ values of eclogitic diamonds compared to peridotitic diamonds has been attributed to fractionation of mantle C during CO_2-escape from a carbonated fluid/melt before diamond formation (Cartigny et al., 2001). This fractionation model, however, is not likely to produce diamonds with $\delta^{13}C < -14$ ‰ from a source with initial mantle-like C isotope compositions (Smart et al., 2011). A more probable source of ^{13}C-depleted C for Koidu eclogitic diamonds is recycled crustal material (Milledge et al., 1983; Kirkley et al., 1991), in particular biogenic carbonate ± organic matter from subducted altered oceanic crust (AOC; Li et al., 2019).

The major reservoirs for crustal C in AOC include normal marine carbonate ($\delta^{13}C$ ~0 ‰; Schidlowski, 2001; Cartigny et al., 2014), ^{13}C-depleted biogenic carbonate ($\delta^{13}C$ as low as -24 ‰;

Li et al., 2019) and organic matter (average $\delta^{13}C$ of -26 ± 7 ‰; Schidlowski, 2001). Similarly, crustal N from clay minerals formed by low-temperature (< 100°C) and high-temperature (> 250°C) alteration of oceanic crust has high $\delta^{15}N$ and low $\delta^{15}N$ values, respectively (Busigny et al., 2005; Li et al., 2019). Devolatilization of C and N from AOC during subduction further decreases $\delta^{13}C$ and increases $\delta^{15}N$ values in the residue (Bebout and Fogel, 1992; Li et al., 2014; Cartigny et al., 2014). Devolatilization and mixing of C and N from these various AOC reservoirs (± a mantle component) can explain the diverse $\delta^{13}C$ and $\delta^{15}N$ values of the eclogitic diamonds contained in Cluster 1 (Fig. 13a).

Cluster 3: Mantle-derived fluids/melts (i.e., fluids/melts that ultimately derive from the convecting upper mantle) associated with kimberlitic or carbonatitic magmatism are invoked for the crystallization of fibrous diamonds (Boyd et al., 1987; Navon et al., 1988; Boyd et al., 1994b). The confined ranges of $\delta^{13}C$ and $\delta^{15}N$ values (both are close to -5 ‰; Boyd et al., 1987; Cartigny, 2005; Cartigny et al., 2014; Petts et al., 2016) in fibrous diamonds worldwide indicate that the mantle reservoir of their parental fluids/melts has homogeneous C and N isotope compositions. The $\delta^{13}C$ and $\delta^{15}N$ values of rocks that are sourced directly from the convecting upper mantle, i.e. fresh mid-ocean ridge basalts (MORB), also fall in similar ranges (Marty and Zimmermann, 1999; Cartigny et al., 2014), suggesting that they are the isotopic signature of the convecting depleted mantle. Thus, Koidu diamonds in Cluster 3, with C and N isotope compositions similar to fibrous diamonds and MORB, likely formed from relatively homogeneous, mantle-derived fluids/melts (Fig. 13b).

The observation that the eclogitic diamond rims fall into “mantle-like” Cluster 3 suggests that the diamond-forming melts/fluids switched from slab-derived to mantle-derived. Decoupling between mineral inclusion composition (related to the eclogitic diamond substrates) and diamond

C and N (derived externally, from deeper portions of a slab and/or the lithospheric or convecting mantle) is common, as revealed by a prominent mode in $\delta^{13}C$ at -5 ‰ and mostly negative $\delta^{15}N$ values for eclogitic inclusion-bearing diamonds worldwide (Cartigny, 2005; Stachel et al., 2009; Cartigny et al., 2014). Although mixed paragenesis diamond 138-7 (in Cluster 3) contains both eclogitic and peridotitic inclusions, none of its growth zones show isotope compositions clearly indicative of subducted C and N, again indicating decoupling between an evolving/changing substrate and the apparently constant source of the diamond-forming fluid.

Cluster 2: Mixing of C and N derived from the convecting mantle with subducted components shifts diamond $\delta^{13}C$ and $\delta^{15}N$ away from the mantle value, following mixing arrays that are controlled in their curvature by the ratio $(N/C)_{Mantle}/(N/C)_{AOC}$ (Li et al., 2019) (Fig. 13a). Almost two-thirds of the diamonds in Cluster 2 have $\delta^{13}C > -4$ ‰ and the majority have positive $\delta^{15}N$ values, possibly reflecting variable degrees of mixing between a mantle-derived component ($\delta^{13}C = -5$ ‰ and $\delta^{15}N = -5$ ‰) and a normal marine carbonate- ($\delta^{13}C \approx 0$ ‰) and low-temperature clay-derived ($\delta^{15}N > 0$ ‰) subducted component (Li et al., 2019). Generally, diamonds showing only minor ^{13}C enrichment relative to the mantle value but strongly variable $\delta^{15}N$ values suggest decoupling of C and N (Mikhail et al., 2014). Alternatively, the slightly ^{13}C-enriched character of Cluster 2 could be a mantle signature unique to the West African Craton, since similar mild shifts to elevated $\delta^{13}C$ values were also observed for peridotitic diamonds from Kankan (Guinea; Stachel et al., 2002) and Akwatia (Ghana; Stachel and Harris, 1997). The observation that this signature extends to lower mantle diamonds from Kankan (Stachel et al., 2002; Palot et al., 2014) may indicate a plume source of mildly ^{13}C-enriched C, possibly ultimately linked to deeply subducted crustal material. The spread in N isotope composition of Cluster 2 could then also be linked to

557 mixing between asthenosphere-derived ($\delta^{15}N$ of -5 ± 2 ‰; Cartigny and Marty, 2013) and plume-
558 derived components ($\delta^{15}N$ of +3 ± 2 ‰; Dauphas and Marty, 1999; Marty and Dauphas, 2003).

559 **6.5 Growth episodes of Koidu diamonds**

560 The three distinct clusters in $\delta^{13}C$–$\delta^{15}N$ space suggest that multiple diamond growth events
561 occurred in the lithospheric mantle beneath Koidu (Fig. 13). Eclogitic diamond cores formed from
562 subducted crustal material (Cluster 1) and rims from mantle-derived fluids/melts (Cluster 3). This
563 sequence indicates eclogitic diamond growth in at least two distinct episodes. One mixed
564 paragenesis diamond (133-6) shows inner growth zones indicative of mixed C and N sources
565 (mantle and subducted; Cluster 2) and a rim that again has a purely mantle-like signature (Cluster
566 3). The abrupt change of isotopic signature between core and rim in these diamonds documents
567 that their growth followed two sequences: Cluster 1 → Cluster 3 and Cluster 2 → Cluster 3, with
568 the temporal relationship between Clusters 1 and 2 remaining unconstrained.

569 Crystallization of the earlier generation of eclogitic diamonds (Cluster 1) may have been
570 coeval with or subsequent to Archean subduction and eclogite emplacement beneath the Man
571 Shield (Barth et al., 2002a; Aulbach et al., 2019a). For eclogitic sulphide-bearing diamonds from
572 nearby Zimmi, Re-Os dating indicated formation only in the Neoproterozoic (~650 Ma; Smit et
573 al., 2016), but involving S that had experienced mass independent isotopic fractionation in the
574 Archean atmosphere (Smit et al., 2019a), thereby documenting an indirect link to Archean
575 subduction processes. Given the subduction signature of Cluster 1 diamonds, their formation likely
576 is associated with C contained within the Archean slab, but an additional fluid/melt pulse may still
577 be required to facilitate mobilization and re-precipitation of the subducted C and to add a mantle-
578 like N component to the compositional array.

A detailed study of Koidu eclogites (Aulbach et al., 2019b) indicated that a subset of diamondiferous low-MgO eclogites and gabbroic eclogites were transformed to barren high-MgO eclogites and pyroxenites as a consequence of metasomatic overprint associated with the Neoproterozoic break-up of Rodinia. The 650 Ma age obtained for Zimmi diamonds (Smit et al., 2016) correlates with the timing of this event. Mixed paragenesis diamonds with a mantle-like stable isotope composition, either throughout (138-7) or in a distinct rim zone (133-6), and the mantle-like composition of the secondary overgrowth on eclogitic diamonds suggest that these metasomatic processes and the transition to diamond formation with mantle-like C and N isotopic signatures may be linked.

We propose that after initial growth of eclogitic diamonds (Cluster 1), there were at least two pulses of metasomatic agents involved in the growth of diamonds, the first resulting in Cluster 2 and the second in Cluster 3. The first pulse of carbonated ultrabasic melt, derived possibly from either a mantle plume or melting initiated by subduction-related fluids, infiltrated eclogite lenses in the lithospheric mantle, converting some low-MgO and gabbroic eclogites to high-MgO eclogites and pyroxenites (Hills and Haggerty, 1989; Barth et al., 2002b). Some of the original diamond content of the low-MgO and gabbroic eclogites may have been destroyed by the infiltrating melt (Aulbach et al., 2019b). The same pulse of carbonated melt also infiltrated surrounding peridotites (possibly evolving into an aqueous CHO fluid upon equilibration with subsolidus harzburgites). This metasomatic event was associated with the precipitation of Cluster 2 diamonds (peridotitic suite and the core of mixed paragenesis diamond 133-6) with mild ^{13}C enrichment and variable ^{15}N enrichment. The trend of outward increasing $\delta^{13}C$ values and decreasing N concentrations in the central portion of diamond 133-6 suggests that this melt pulse

601 was relatively oxidizing (Fig. 11), driven by carbonate reduction, or redox-neutral precipitation
602 from coexisting CH_4 and CO_2 during cooling.

603 A second pulse of melt/fluid with an asthenosphere-derived C and N isotope signature
604 infiltrated the local lithospheric mantle after a significant period of time, documented by the
605 different N aggregation states of cores and rims of some diamonds (Fig. 12). This pulse was more
606 N-rich and a lack of covariation between $\delta^{13}C$ values and N abundance in precipitated Cluster 3
607 diamonds indicates that fluid-limited conditions did not occur. Infiltration of this melt/fluid is
608 documented in the rims of eclogitic diamonds and some mixed paragenesis diamonds (133-6 (rim)
609 and 138-7).

610 The two instances of peridotitic inclusions in the rims of mixed paragenesis diamonds are
611 both related to this second metasomatic event, based on mantle-like $\delta^{13}C$ and $\delta^{15}N$ values and high
612 N contents of these diamond growth zones. As discussed above, the earlier eclogitic and later
613 peridotitic inclusions in the studied mixed paragenesis diamonds have the respective chemical
614 signatures of eclogitic and peridotitic mantle xenolith minerals, requiring that the diamonds
615 involved must have physically moved between different diamond substrates. Infiltration of an
616 eclogite-derived fluid into a peridotitic diamond substrate (Mikhail et al. 2021) is neither consistent
617 with the clearly crust-derived signatures of the eclogitic inclusions nor with the very Mg- and Cr-
618 rich character of the peridotitic inclusions. Physical transport may have been associated with melt
619 injection, as documented by polymict mantle breccias (juxtaposition of minerals and rock clasts
620 from strongly disparate lithologies) observed as xenoliths from the Kaapvaal craton (Zhang et al.,
621 2003; Giuliani et al., 2014). Alternatively, intense deformation involving small eclogite bodies
622 may have achieved transport of resistant minerals such as diamond into surrounding peridotite
623 along high-strain shear zones. Partial melting of eclogites during fluid influx (Spetsius, 1998) and

segregation of such melts may also have allowed for physical transport of originally eclogitic diamonds into peridotitic substrates, followed by renewed diamond growth and encapsulation of peridotitic minerals (Wang, 1998). As indicated by a mild resorption boundary within the one mixed paragenesis diamond entirely associated with Cluster 3 (138-7), this second fluid/melt infiltration may have occurred as repeated pulses over an extended period of time.

7. Conclusions

Combined C and N isotope composition of diamond is a robust tracer of the source of diamond-forming fluids/melts. The distinct isotopic signatures, CL responses and N aggregation states observed in the cores and rims of Koidu diamonds suggest episodic diamond growth during multiple pulses of melts/fluids. In their stable isotope compositions, Koidu diamonds of peridotitic, eclogitic and mixed paragenesis form three major clusters: Cluster 1 (cores of eclogitic diamonds) has low $\delta^{13}C$ and highly variable $\delta^{15}N$ values ($\delta^{13}C$ = -33.2 to -14.4 ‰; $\delta^{15}N$ = -5.3 to +10.1 ‰), suggesting derivation from recycled crustal material (± a mantle component). Cluster 2 (peridotitic diamonds and core of mixed paragenesis diamond 133-6) has mantle-like to mildly ^{13}C-enriched C isotope compositions and a wide range of $\delta^{15}N$ values ($\delta^{13}C$ = -6.0 to -1.1 ‰; $\delta^{15}N$ = -4.2 to +9.7 ‰), likely reflecting mixing of C and N from subducted and mantle sources. Cluster 3 (rims of eclogitic diamonds and of mixed paragenesis diamond 133-6, and mixed paragenesis diamond 138-7) has a homogeneous isotopic signature similar to fibrous diamonds and MORB ($\delta^{13}C$ = -7.8 to -3.6 ‰; $\delta^{15}N$ = -7.9 to -2.1 ‰), pointing to precipitation from mantle-derived fluids/melts. Transects across mixed paragenesis diamond 133-6 indicate that the fluid/melt pulse responsible for the growth of its innermost zones (Cluster 2) was relatively oxidizing (gradual outward increase in $\delta^{13}C$ and decrease in N), whereas diamonds in Clusters 1 and 3 likely precipitated in systems

that were not fluid-limited, precluding isotopic fractionation, and thus the redox states of their growth media cannot be constrained.

Mixed paragenesis diamonds are associated with all three clusters (1, 2 and 3), but the two examples where we could document a transition from an eclogitic paragenesis core to a peridotitic paragenesis rim either show a transition from mixed source-type Cluster 2 (core) to mantle-like Cluster 3 (rim) or fall entirely into Cluster 3. Based on the major and trace element composition of the mineral inclusions in these mixed paragenesis diamonds, which provide good matches to the equivalent minerals in a subset of Koidu eclogites and in cratonic peridotites, we exclude precipitation during a single intense metasomatic event but instead invoke physical transport of diamonds from eclogitic to peridotitic substrates between separate growth events. The highly depleted character of the peridotitic inclusions precludes that diamond transport involved significant interaction between the peridotitic substrates and either eclogite or melt, which favours either mechanical shearing of small eclogite pods residing in lithospheric peridotites or diamond transport and injection into peridotite through small melt volumes.

Acknowledgments

MYL acknowledges support through a NSERC CREATE (DERTS) funding. TS and DGP acknowledge support through NSERC Discovery grant funding. We thank Andrew Locock and Yan Luo for help with EPMA and LA-ICP-MS, respectively, and Robert Dokken for mount preparation and imaging for SIMS analyses. We thank Sonja Aulbach, Oded Navon and Sami Mikhail for thorough reviews and constructive comments that greatly improved the paper, as well as Dmitri Ionov for efficient editorial handling.

Appendix A. Supplementary Material

Characteristics of Koidu diamonds are shown in Table S1. Data of FTIR analysis of Koidu diamond 128-7 are shown in Table S2. Major element compositions of mineral inclusions in other Koidu mixed paragenesis diamonds are shown in Table S3. Data of SIMS analysis of Koidu diamonds are shown in Table S4. Examples of common surface textures observed in Koidu diamonds are shown in Fig. S1.

References

Aulbach S. and Jacob D. E. (2016) Major- and trace-elements in cratonic mantle eclogites and pyroxenites reveal heterogeneous sources and metamorphic processing of low-pressure protoliths. *Lithos* **262**, 586–605.

Aulbach S., Stachel T., Viljoen K. S., Brey G. P. and Harris J. W. (2002) Eclogitic and websteritic diamond sources beneath the Limpopo Belt - Is slab-melting the link? *Contrib. to Mineral. Petrol.* **143**, 56–70.

Aulbach S., Pearson N. J., O'Reilly S. Y., and Doyle B. J. (2007) Origins of xenolithic eclogites and pyroxenites from the Central Slave Craton, Canada. *J. Petrol*. **48**, 1843–1873.

Aulbach S., Jacob D. E., Cartigny P., Stern R. A., Simonetti S. S., Wörner G., and Viljoen K. S. (2017) Eclogite xenoliths from Orapa: ocean crust recycling, mantle metasomatism and carbon cycling at the western Zimbabwe craton margin. *Geochim. Cosmochim. Acta* **213**, 574-592.

690 Aulbach S., Heaman L. M., Jacob D. E., and Viljoen K. S. (2019a) Ages and sources of mantle
691 eclogites: ID-TIMS and in situ MC-ICPMS Pb-Sr isotope systematics of
692 clinopyroxene. *Chem. Geol.* **503**, 15–28.

693 Aulbach S., Höfer H. E. and Gerdes A. (2019b) High-Mg and Low-Mg Mantle eclogites from
694 Koidu (West African Craton) linked by neoproterozoic ultramafic melt metasomatism of
695 subducted archaean plateau-like oceanic crust. *J. Petrol.* **60**, 723–754.

696 Barth M. G., Rudnick R. L., Horn I., McDonough W. F., Spicuzza M. J., Valley J. W. and
697 Haggerty S. E. (2001) Geochemistry of xenolithic eclogites from West Africa, part I: A link
698 between low MgO eclogites and archean crust formation. *Geochim. Cosmochim. Acta* **65**,
699 1499–1527.

700 Barth M. G., Rudnick R. L., Carlson R. W., Horn I. and McDonough W. F. (2002a) Re-Os and
701 U-Pb geochronological constraints on the eclogite-tonalite connection in the Archean Man
702 Shield, West Africa. *Precambrian Res.* **118**, 267–283.

703 Barth M. G., Rudnick R. L., Horn I., McDonough W. F., Spicuzza M. J., Valley J. W. and
704 Haggerty S. E. (2002b) Geochemistry of xenolithic eclogites from West Africa, part 2:
705 origins of the high MgO eclogites. *Geochim. Cosmochim. Acta* **66**, 4325–4345.

706 Bebout G. E. and Fogel M. L. (1992) Nitrogen-isotope compositions of metasedimentary rocks
707 in the Catalina Schist, California: implications for metamorphic devolatilization history.
708 *Geochim. Cosmochim. Acta* **56**, 2839–2849.

709 Boyd S. R., Mattey D. P., Pillinger C. T., Milledge H. J., Mendelssohn M. and Seal M. (1987)
710 Multiple growth events during diamond genesis: an integrated study of carbon and nitrogen
711 isotopes and nitrogen aggregation state in coated stones. *Earth Planet. Sci. Lett.* **86**, 341–

353.

Boyd S. R., Kiflawi I. and Woods G. S. (1994a) The relationship between infrared absorption and the A defect concentration in diamond. *Philos. Mag. B* **69**, 1149–1153.

Boyd S. R., Pineau F. and Javoy M. (1994b) Modelling the growth of natural diamonds. *Chem. Geol.* **116**, 29–42.

Boyd S. R., Kiflawi I. and Woods G. S. (1995) Infrared absorption by the B nitrogen aggregate in diamond. *Philos. Mag. B* **72**, 351–361.

Busigny V., Laverne C. and Bonifacie M. (2005) Nitrogen content and isotopic composition of oceanic crust at a superfast spreading ridge: A profile in altered basalts from ODP Site 1256, Leg 206. *Geochemistry, Geophys. Geosystems* **6**, 1–16.

Cartigny P. (2005) Stable isotopes and the origin of diamond. *Elements* **1**, 79–84.

Cartigny P. and Marty B. (2013) Nitrogen isotopes and mantle geodynamics: the emergence of life and the atmosphere-crust-mantle connection. *Elements* **9**, 359–366.

Cartigny P., Harris J. W. and Javoy M. (2001) Diamond genesis, mantle fractionations and mantle nitrogen content: a study of δ13C-N concentrations in diamonds. *Earth Planet. Sci. Lett.* **185**, 85–98.

Cartigny P., Palot M., Thomassot E. and Harris J. W. (2014) Diamond formation: a stable isotope perspective. *Annu. Rev. Earth Planet. Sci.* **42**, 699–732.

Clark J. R. and Papike J. J. (1968) Crystal-chemical characterization of omphacites. *Am. Mineral.* **53**, 840–868.

Coplen T.B., Böhlke J.K., De Bievre P., Ding T., Holden N.E., Hopple J.A., Krouse H.R.,

733 Lamberty A., Peiser H.S., Revesz K. and Rieder S.E. (2002) Isotope-abundance variations
734 of selected elements (IUPAC Technical Report). *Pure Appl. Chem.* **74**, 1987–2017.

735 Dauphas N. and Marty B. (1999) Heavy nitrogen in carbonatites of the Kola Peninsula: a
736 possible signature of the deep mantle. *Science.* **286**, 2488–2490.

737 Davies G. (1976) The A nitrogen aggregate in diamond-its symmetry and possible structure. *J.*
738 *Phys. C Solid State Phys.* **9**, L537–L542.

739 Davies R. M., Griffin W. L., O'Reilly S. Y. and Andrew A. S. (2003) Unusual mineral inclusions
740 and carbon isotopes of alluvial diamonds from Bingara, eastern Australia. *Lithos* **69**, 51–66.

741 Davies R. M., Griffin W. L., O'Reilly S. Y. and McCandless T. E. (2004a) Inclusions in
742 diamonds from the K14 and K10 kimberlites, Buffalo Hills, Alberta, Canada: Diamond
743 growth in a plume? *Lithos* **77**, 99–111.

744 Davies R. M., Griffin W. L., O'Reilly S. Y. and Doyle B. J. (2004b) Mineral inclusions and
745 geochemical characteristics of microdiamonds from the DO27, A154, A21, A418, DO18,
746 DD17 and Ranch Lake kimberlites at Lac de Gras, Slave Craton, Canada. *Lithos* **77**, 39–55.

747 Deines P. (1980) The carbon isotopic composition of diamonds: relationship to diamond shape,
748 color, occurrence and vapor composition. *Geochim. Cosmochim. Acta* **44**, 943–961.

749 Deines P. and Harris J. W. (1995) Sulfide inclusion chemistry and carbon isotopes of African
750 diamonds. *Geochim. Cosmochim. Acta* **59**, 3173–3188.

751 Fung A. T. and Haggerty S. E. (1995) Petrography and mineral compositions of eclogites from
752 the Koidu Kimberlite Complex, Sierra Leone. *J. Geophys. Res.* **100**.

753 Giuliani, A., Phillips, D., Kamenetsky, V. S., Kendrick, M. A., Wyatt, B. A., Goemann, K. and

754 Hutchinson, G. (2014) Petrogenesis of mantle polymict breccias: insights into mantle
755 processes coeval with kimberlite magmatism. *J. Petrol.* **55**, 831-858.

756 Green T. H. (1994) Experimental studies of trace-element partitioning applicable to igneous
757 petrogenesis - Sedona 16 years later. *Chem. Geol.* **117**, 1–36.

758 Hall A. E. and Smith C. B. (1984) Lamproite diamonds - Are they different? *Univ. West. Aust.*
759 *Dep. Geol. Publ.* **8**, 167–212.

760 Harder M., Nowicki T. E., Hetman C. M., Freeman L. and Abedu B. (2013) Geology and
761 Evaluation of the K2 Kimberlite, Koidu Mine, Sierra Leone, West Africa. *Proc. 10th Int.*
762 *Kimberl. Conf.*, 191–208.

763 Harte B., and Kirkley M. B. (1997) Partitioning of trace elements between clinopyroxene and
764 garnet: data from mantle eclogites. *Chem. Geol.* **136**, 1-24.

765 Hills D. V. and Haggerty S. E. (1989) Petrochemistry of eclogites from the Koidu Kimberlite
766 Complex, Sierra Leone. *Contrib. to Mineral. Petrol.* **103**, 397–422.

767 Howell D., O'Neill C. J., Grant K. J., Griffin W. L., Pearson N. J. and O'Reilly S. Y. (2012) μ-
768 FTIR mapping : Distribution of impurities in different types of diamond growth. *Diam.*
769 *Relat. Mater.* **29**, 29–36.

770 Ireland T. R., Rudnick R. L. and Spetsius Z. (1994) Trace elements in diamond inclusions from
771 eclogites reveal link to Archean granites. *Earth Planet. Sci. Lett.* **128**, 199–213.

772 Jacob D. E. (2004) Nature and origin of eclogite xenoliths from kimberlites. *Lithos* **77**, 295–316.

773 Jaques A., Hall A., Sheraton J., Smith C., Sun S.-S., Drew R., Foudoulis C. and Ellingsen K.
774 (1989) Composition of crystalline inclusions and C-isotopic composition of Argyle and

Ellendale diamonds. *Ross J, al. Kimberlites Relat. rocks GSA Spec Publ 14, vol 2. Blackwell, Carlt.*, 966–989.

Jochum K. P., Nohl U., Herwig K., Lammel E., Stoll B., and Hofmann A. W. (2005) GeoReM: a new geochemical database for reference materials and isotopic standards. *Geostand. Geoanal. Res.* **29**, 333–338.

Jones R., Briddon P. R. and Öberg S. (1992) First-principles theory of nitrogen aggregates in diamond. *Philos. Mag. Lett.* **66**, 67–74.

Junk G. and Svec H. J. (1958) The absolute abundance of the nitrogen isotopes in the atmosphere and compressed gas from various sources. *Geochim. Cosmochim. Acta* **14**, 234–243.

Kirkley M. B., Gurney J. J., Otter M. L., Hill S. J. and Daniels L. R. (1991) The application of C isotope measurements to the identification of the sources of C in diamonds: a review. *Appl. Geochemistry* **6**, 477–494.

Klein-BenDavid O., Logvinova A. M., Schrauder M., Spetius Z. V., Weiss Y., Hauri E. H., Kaminsky F. V., Sobolev N. V. and Navon O. (2009) High-Mg carbonatitic microinclusions in some Yakutian diamonds-a new type of diamond-forming fluid. *Lithos* **112S**, 648–659.

Leahy K. and Taylor W. R. (1997) The influence of the Glennie domain deep structure on the diamonds in Saskatchewan kimberlites. *Geol. i Geofiz.* **38**, 451–460.

Li K., Li L., Pearson D. G. and Stachel T. (2019) Diamond isotope compositions indicate altered igneous oceanic crust dominates deep carbon recycling. *Earth Planet. Sci. Lett.* **516**, 190–201.

Li L., Zheng Y. F., Cartigny P. and Li J. (2014) Anomalous nitrogen isotopes in ultrahigh-

796 pressure metamorphic rocks from the Sulu orogenic belt: Effect of abiotic nitrogen
797 reduction during fluid-rock interaction. *Earth Planet. Sci. Lett.* **403**, 67–78.

798 Mallik A. and Dasgupta R. (2012) Reaction between MORB-eclogite derived melts and fertile
799 peridotite and generation of ocean island basalts. *Earth Planet. Sci. Lett.* **329**–**330**, 97–108.

800 Mallik A. and Dasgupta R. (2013) Reactive infiltration of MORB-eclogite-derived carbonated
801 silicate melt into fertile peridotite at 3 GPa and genesis of alkalic magmas. *J. Petrol.* **54**,
802 2267–2300.

803 Marty B. and Zimmermann L. (1999) Volatiles (He, C, N, Ar) in mid-ocean ridge basalts:
804 Assessment of shallow-level fractionation and characterization of source composition.
805 *Geochim. Cosmochim. Acta* **63**, 3619–3633.

806 Marty B. and Dauphas N. (2003) The nitrogen record for crust-mantle interaction and mantle
807 convection from Archean to present. *Earth Planet. Sci. Lett.* **206**, 397–410.

808 McDonough W. F. and Sun S. S. (1995) The composition of the Earth. *Chem. Geol.* **120**, 223–
809 253.

810 McDonough W. F. and Rudnick R. L. (1998) Mineralogy and composition of the upper mantle.
811 *Rev. Mineral.* **37**, 139–164.

812 Meyer H. O. A. (1987) Inclusions in diamond. *Nixon PH Mantle xenoliths, John Wiley Sons,*
813 *Chichester*, 501–522.

814 Meyer H. O. A. and Boyd F. R. (1972) Composition and origin of crystalline inclusions in
815 natural diamonds. *Geochim. Cosmochim. Acta* **36**, 1255–1273.

816 Mikhail S., Verchovsky A. B., Howell D., Hutchison M. T., Southworth R., Thomson A. R.,

Warburton P., Jones A. P. and Milledge H. J. (2014) Constraining the internal variability of the stable isotopes of carbon and nitrogen within mantle diamonds. *Chem. Geol.* **366**, 14–23.

Mikhail S., Rinaldi M., Mare E. R. and Sverjensky D. A. (2021) A genetic metasomatic link between eclogitic and peridotitic diamond inclusions. *Geochemical Perspect. Lett.* **17**, 33–38.

Milledge H. J., Mendelssohn M. J., Seal M., Rouse J. E., Swart P. K. and Pillinger C. T. (1983) Carbon isotopic variation in spectral type II diamonds. *Nature* **303**, 791–792.

Moore R. O. and Gurney J. J. (1986) Mineral inclusions in diamonds from the Monastery kimberlite, South Africa. *Int. Kimberl. Conf. Ext. Abstr.* **4**, 406–408.

Navon O., Hutcheon I. D., Rossman G. R. and Wasserburg G. J. (1988) Mantle-derived fluids in diamond micro-inclusions. *Nature* **335**, 784–789.

Otter M. L. and Gurney J. J. (1986) Mineral inclusions in diamonds from the Sloan diatremes, Colorado-Wyoming State Line kimberlite district, North America. *Int. Kimberl. Conf. Ext. Abstr.* **4**, 415–417.

Palot M., Pearson D. G., Stern R. A., Stachel T., and Harris J. W. (2014) Isotopic constraints on the nature and circulation of deep mantle C–H–O–N fluids: Carbon and nitrogen systematics within ultra-deep diamonds from Kankan (Guinea). *Geochim. Cosmochim. Acta* **139**, 26-46.

Petts D. C., Chacko T., Stachel T., Stern R. A. and Heaman L. M. (2015) A nitrogen isotope fractionation factor between diamond and its parental fluid derived from detailed SIMS

analysis of a gem diamond and theoretical calculations. *Chem. Geol.* **410**, 188–200.

Petts D. C., Stachel T., Stern R. A., Hunt L. and Fomradas G. (2016) Multiple carbon and nitrogen sources associated with the parental mantle fluids of fibrous diamonds from Diavik, Canada, revealed by SIMS microanalysis. *Contrib. to Mineral. Petrol.* **171**, 1–15.

Prinz M., Vincent Manson D., Hlava P. F. and Keil K. (1975) Inclusions in diamonds: Garnet lherzolite and eclogite assemblages. *Phys. Chem. Earth* **9**, 797–815.

Rollinson H. (2016) Archaean crustal evolution in West Africa: a new synthesis of the Archaean geology in Sierra Leone, Liberia, Guinea and Ivory Coast. *Precambrian Res.* **281**, 1–12.

Schidlowski M. (2001) Carbon isotopes as biogeochemical recorders of life over 3.8 Ga of earth history: evolution of a concept. *Precambrian Res.* **106**, 117–134.

Schmickler B., Jacob D. E. and Foley S. F. (2004) Eclogite xenoliths from the Kuruman kimberlites, South Africa: geochemical fingerprinting of deep subduction and cumulate processes. *Lithos* **75**, 173–207.

Shu Q., Brey G. P., Hoefer H. E., Zhao Z. and Pearson D. G. (2016) Kyanite/corundum eclogites from the Kaapvaal Craton: subducted troctolites and layered gabbros from the Mid- to Early Archean. *Contrib. to Mineral. Petrol.* **171**, 1–24.

Skinner E. M. W., Apter D. B., Morelli C. and Smithson N. K. (2004) Kimberlites of the Man craton, West Africa. *Lithos* **76**, 233–259.

Smart K. A., Chacko T., Stachel T., Muehlenbachs K., Stern R. A. and Heaman L. M. (2011) Diamond growth from oxidized carbon sources beneath the Northern Slave Craton, Canada: a δ13C-N study of eclogite-hosted diamonds from the Jericho kimberlite. *Geochim.*

Cosmochim. Acta **75**, 6027–6047.

Smit K. V., Shirey S. B. and Wang W. (2016) Type Ib diamond formation and preservation in the West African lithospheric mantle: Re–Os age constraints from sulphide inclusions in Zimmi diamonds. *Precambrian Res.* **286**, 152–166.

Smit K. V., Shirey S. B., Hauri E. H. and Stern R. A. (2019a) Sulfur isotopes in diamonds reveal differences in continent construction. *Science* **364**, 383–385.

Smit K. V., Stachel T., Luth R. W. and Stern R. A. (2019b) Evaluating mechanisms for eclogitic diamond growth: An example from Zimmi Neoproterozoic diamonds (West African craton). *Chem. Geol.* **520**, 21–32.

Sobolev N. V., Snyder G. A., Taylor L. A., Keller R. A., Yefimova E. S., Sobolev V. N. and Shimizu N. (1998) Extreme chemical diversity in the mantle during eclogitic diamond formation: Evidence from 35 garnet and 5 pyroxene inclusions in a single diamond. *Int. Geol. Rev.* **40**, 567–578.

Spetsius Z. V. (1998) Two generations of diamonds in eclogitic xenoliths from Yakutia. *Proc. 7th Int. Kimberl. Conf.*, 844–846.

Stachel T. and Harris J. W. (1997) Syngenetic inclusions in diamond from the Birim field (Ghana) - A deep peridotitic profile with a history of depletion and re-enrichment. *Contrib. to Mineral. Petrol.* **127**, 336–352.

Stachel T. and Harris J. W. (2008) The origin of cratonic diamonds — Constraints from mineral inclusions. *Ore Geol. Rev.* **34**, 5–32.

Stachel T., Harris J. W. and Brey G. P. (1998) Rare and unusual mineral inclusions in diamonds

from Mwadui, Tanzania. *Contrib. to Mineral. Petrol.* **132**, 34–47.

Stachel T., Harris J. W., Brey G. P. and Joswig W. (2000a) Kankan diamonds (Guinea) II: lower mantle inclusion parageneses. *Contrib. to Mineral. Petrol.* **140**, 16–27.

Stachel T., Brey G. P. and Harris J. W. (2000b) Kankan diamonds (Guinea) I: From the lithosphere down to the transition zone. *Contrib. to Mineral. Petrol.* **140**, 1–15.

Stachel T., Harris J. W., Aulbach S. and Deines P. (2002) Kankan diamonds (Guinea) III: $\delta^{13}C$ and nitrogen characteristics of deep diamonds. *Contrib. to Mineral. Petrol.* **142**, 465–475.

Stachel T., Aulbach S., Brey G. P., Harris J. W., Leost I., Tappert R. and Viljoen K. S. (2004) The trace element composition of silicate inclusions in diamonds: a review. *Lithos* **77**, 1–19.

Stachel T., Harris J. W. and Muehlenbachs K. (2009) Sources of carbon in inclusion bearing diamonds. *Lithos* **112S**, 625–637.

Stachel T., Chacko T. and Luth R. W. (2017) Carbon isotope fractionation during diamond growth in depleted peridotite: counterintuitive insights from modelling water-maximum CHO fluids as multi-component systems. *Earth Planet. Sci. Lett.* **473**, 44–51.

Stachel T., Aulbach S. and Harris J. W. (2022) Mineral inclusions in lithospheric diamonds. *Rev. Mineral. Geochem.* (in press). https://doi.org/10.7939/DVN/EJUE1G

Stern R. A., Palot M., Howell D., Stachel T., Pearson D. G., Cartigny P. and Oh A. (2014) Methods and reference materials for SIMS diamond C- and N-isotope analysis: Canadian Centre for Isotopic Microanalysis, Research Report 14-01. *Univ. Alberta, Educ. Res. Arch.*

Sun J., Rudnick R. L., Kostrovitsky S., Kalashnikova T., Kitajima K., Li R. and Shu Q. (2020) The origin of low-MgO eclogite xenoliths from Obnazhennaya kimberlite, Siberian craton.

Contrib. to Mineral. Petrol. **175**, 1–22.

Taylor L. A. and Anand M. (2004) Diamonds: Time capsules from the Siberian mantle. *Chemie der Erde* **64**, 1–74.

Taylor W. R., Jaques A. L. L. and Ridd M. (1990) Nitrogen-defect aggregation characteristics of some Australasian diamonds: time-temperature constraints on the source regions of pipe and alluvial diamonds. *Am. Mineral.* **75**, 1290–1310.

Taylor W. R., Canil D. and Milledge H. J. (1996) Kinetics of Ib to IaA nitrogen aggregation in diamond. *Geochim. Cosmochim. Acta* **60**, 4725–4733.

Thomassot E., Cartigny P., Harris J. W. and Viljoen K. S. (2007) Methane-related diamond crystallization in the Earth's mantle: stable isotope evidences from a single diamond-bearing xenolith. *Earth Planet. Sci. Lett.* **257**, 362–371.

Tompkins L. A. and Haggerty S. E. (1984) *The Koidu kimberlite complex, Sierra Leone: geological setting, petrology and mineral chemistry.*, Elsevier Science Publishers B.V.

Vasil'ev E. A., Ivanov-Omskii V. I., Pomazanskii B. S. and Bogush I. N. (2004) The N3 center luminescence quenched by nitrogen impurity in natural diamond. *Tech. Phys. Lett.* **30**, 802–803.

Wang W. (1998) Formation of diamond with mineral inclusions of "mixed" eclogite and peridotite paragenesis. *Earth Planet. Sci. Lett.* **160**, 831–843.

Westerlund K. J. and Gurney J. J. (2004) Silicate and oxide inclusion characteristics and infra-red absorption analysis of diamonds from the Klipspringer kimberlites, South Africa. *South African J. Geol.* **107**, 131–146.

922 Woods G. S. (1986) Platelets and the infrared absorption of Type Ia diamonds. *Proc. R. Soc. A*
923 *Math. Phys. Eng. Sci.* **407**, 219–238.

924 Zaitsev A. M. (2001) *Optical Properties of Diamond: a data handbook.* Springer Berlin
925 Heidelberg, pp 502.

926 Zhang H. F., Menzies M. A. and Mattey D. (2003) Mixed mantle provenance: diverse garnet
927 compositions in polymict peridotites, Kaapvaal craton, South Africa. *Earth Planet. Sci. Lett.*
928 **216**, 329–346.

929

Table 1. Major element (wt%) compositions of mineral inclusions in diamond 133-6 and 138-7.

Sample	133-6*	133-6-4	138-7-1	138-7-2	138-7-3	138-7-4	138-7-6	138-7-7
Mineral	omphacite	Mg-chromite	garnet	garnet	garnet	garnet	garnet	olivine
Paragenesis	E	P	E	E	E	E	E	P
SiO_2	55.75	< 0.02	40.97	41.85	41.00	39.46	40.26	41.98
TiO_2	0.26	0.06	0.45	0.45	0.47	0.47	0.47	< 0.02
Al_2O_3	18.94	7.32	23.21	21.94	22.98	23.86	23.27	< 0.02
Cr_2O_3	0.01	64.46	0.04	0.04	0.02	0.03	0.02	0.07
FeO^{total}	1.93	12.96	9.60	9.56	8.99	8.95	9.11	5.51
NiO	0.03	0.08	< 0.02	< 0.02	< 0.02	0.01	0.01	0.35
MnO	0.02	0.16	0.17	0.18	0.16	0.17	0.16	0.08
MgO	4.96	13.66	9.28	9.70	8.47	8.07	8.36	53.47
CaO	8.65	< 0.02	16.89	16.70	18.55	19.26	19.28	0.02
Na_2O	8.33	< 0.02	0.18	0.17	0.18	0.18	0.18	< 0.02
K_2O	0.22	< 0.02	< 0.02	< 0.02	< 0.02	< 0.02	< 0.02	< 0.02
Total	99.10	98.70	100.79	100.56	100.82	100.46	101.12	101.48
Mg#	82.2	65.2	63.2	64.4	62.7	61.7	62.1	94.5
Ca#			45.1	44.2	49.5	51.2	50.5	

Mg# = 100×Mg/(Mg+Fe); Ca# = 100×Ca/(Ca+Mg+Fe+Mn).

* Average values of multiple omphacites in diamond 133-6 are reported here.

Table 2. Trace element (ppm) compositions of mineral inclusions in diamond 133-6 and 138-7.

Sample	133-6-1	133-6-2	133-6-3	138-7-1	138-7-3	138-7-6
Mineral	Omphacite	Omphacite	Omphacite	Garnet	Garnet	Garnet
La	2.988	3.000	3.016	0.092	0.062	0.062
Ce	4.480	4.642	4.622	0.644	0.559	0.615
Pr	0.315	0.321	0.317	0.203	0.213	0.215
Nd	0.800	0.827	0.870	2.050	1.910	2.090
Sm	0.154	0.142	0.140	1.300	1.314	1.392
Eu	0.059	0.060	0.069	0.716	0.617	0.854
Gd	0.067	0.088	0.100	1.970	2.240	2.440
Tb	0.005	0.008	0.008	0.373	0.321	0.468
Dy	0.050	0.030	0.027	2.770	2.138	3.120
Ho	0.002	0.006	0.006	0.614	0.540	0.660
Er	0.010	0.009	0.005	1.740	1.646	1.715
Tm	n.d.	n.d.	n.d.	0.252	0.182	0.234
Yb	n.d.	0.005	n.d.	1.470	1.116	1.414
Lu	n.d.	n.d.	n.d.	0.198	0.155	0.201
Sc	1.330	1.560	1.680	41.3	36.1	38.4
Ti	1553	1613	1618	2596	2889	2895
V	108	110	110	86.4	78.5	82.5
Ni	326	321	328	78.3	60.2	65.0
Rb	0.540	0.532	0.510	n.d.	n.d.	n.d.
Sr	135	134	133	5.97	4.02	4.05
Y	0.107	0.116	0.097	15.3	14.5	16.6
Zr	2.2	2.2	2.3	12.2	7.1	12.1
Nb	1.120	1.088	1.106	0.091	0.106	0.142
Ba	0.380	0.685	0.628	n.d.	n.d.	n.d.
Hf	0.137	0.131	0.158	0.233	0.146	0.251

n.d. = not determined.

Three omphacites (from diamond 133-6) and three eclogitic garnets (from diamond 138-7) with larger grain size were analyzed.

Table 3. Summary of SIMS analysis of Koidu diamonds.

Paragenesis	No. of diamond	$\delta^{13}C_{VPDB}$ (‰)	[N] (at.ppm)	$\delta^{15}N_{Air}$ (‰)
Peridotitic	18	-6.0 to -1.1	0.4 to 920	-4.2 to +9.7
Eclogitic	82	-33.2 to -0.04	0.4 to 2200	-7.9 to +10.1
Mixed	5	-24.8 to -1.3	0.3 to 1050	-9.8 to +5.8

Figure 1

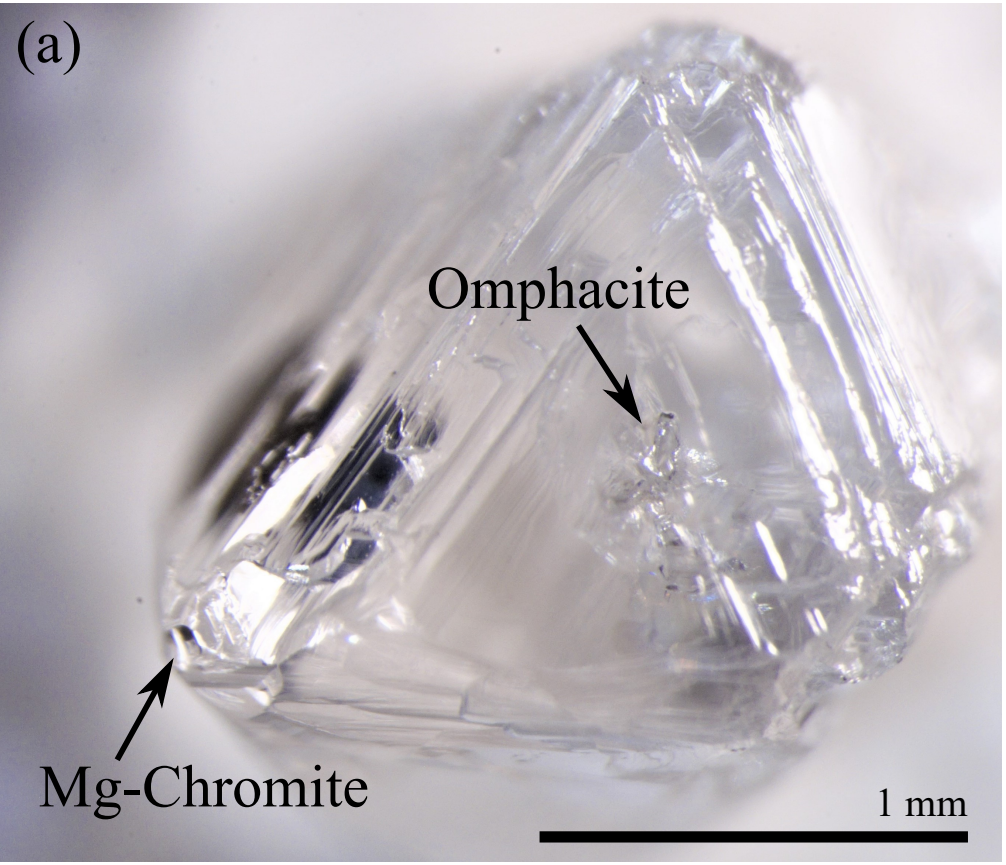

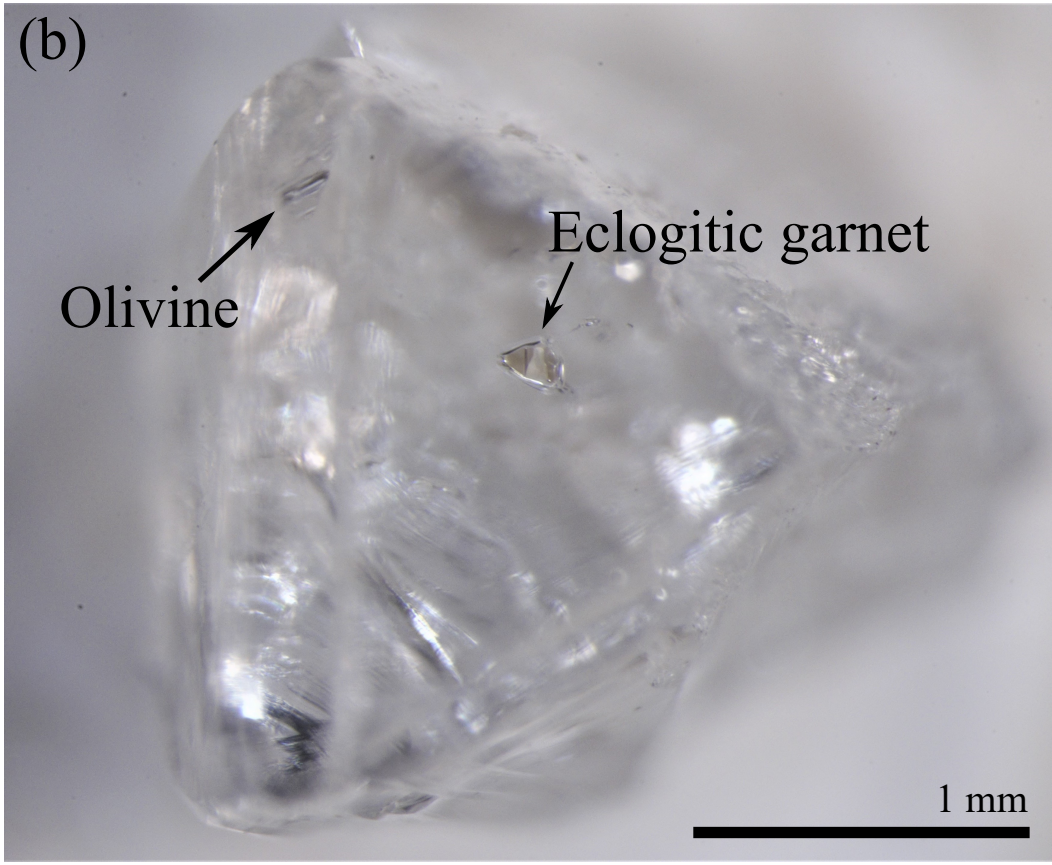

Figure 2

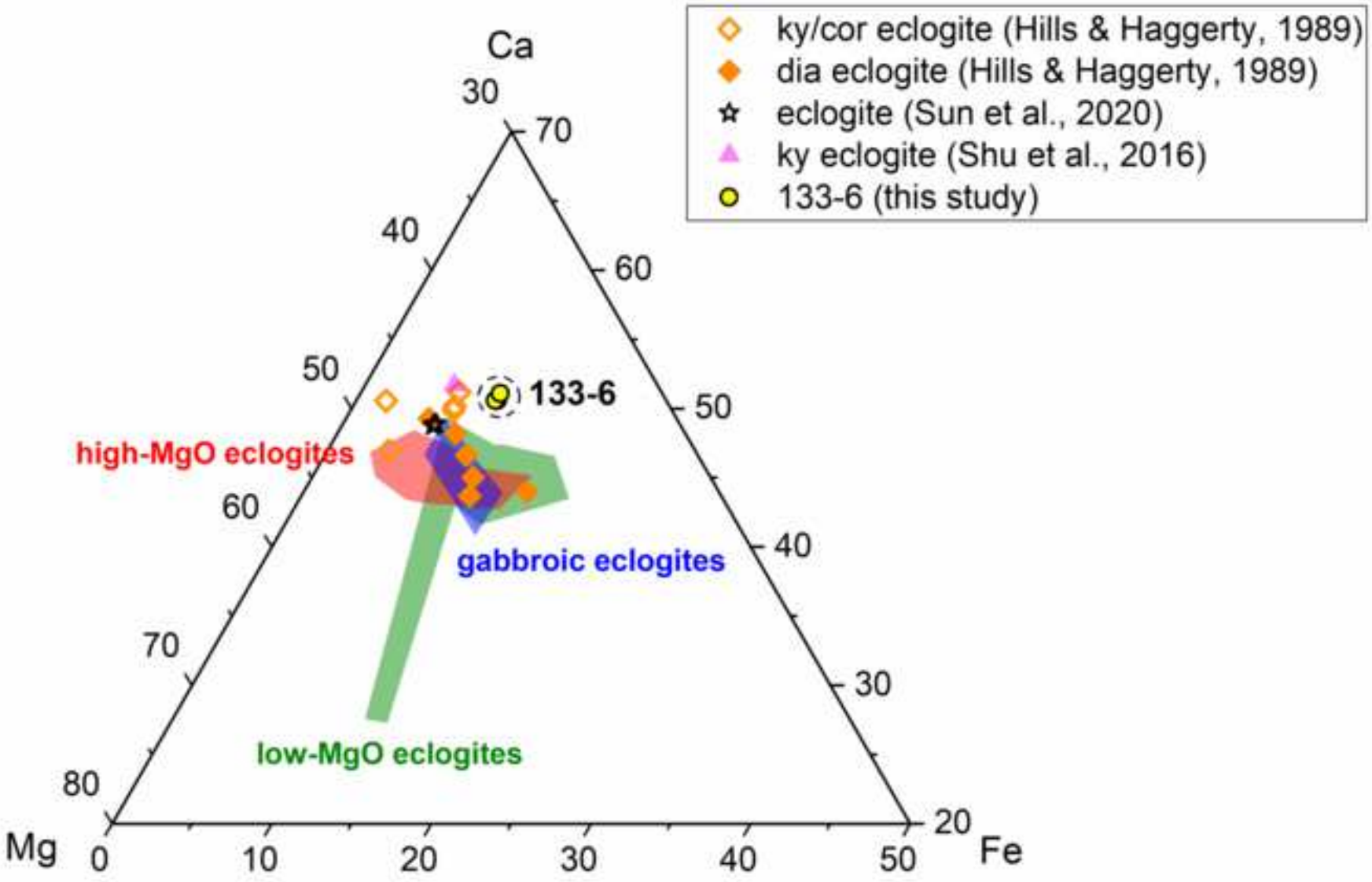

Figure 3

Click here to access/download;Figure;Figure 3_revised.tif

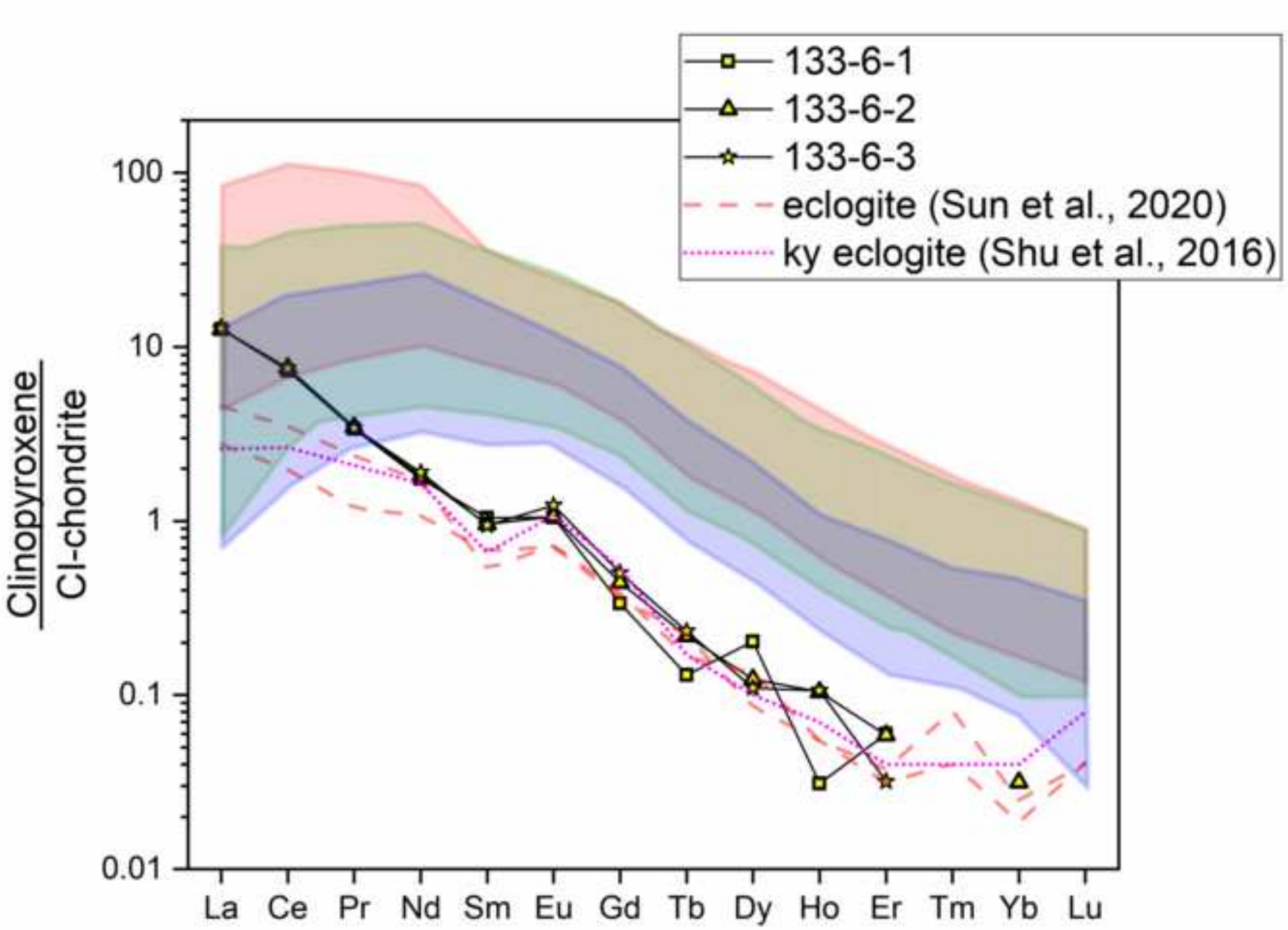

Figure 4

Click here to access/download;Figure;Figure 4_revised.tif

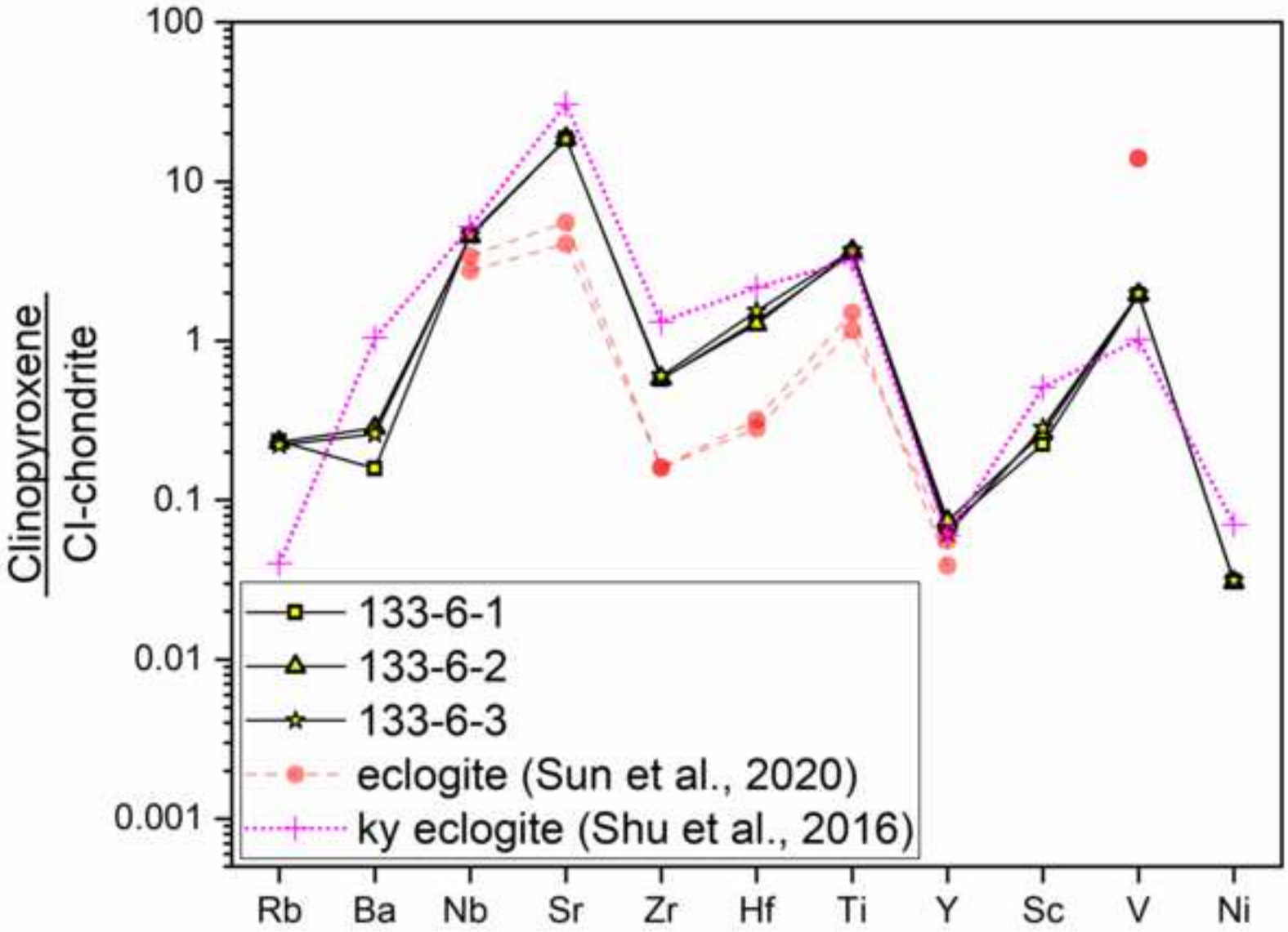

Figure 5

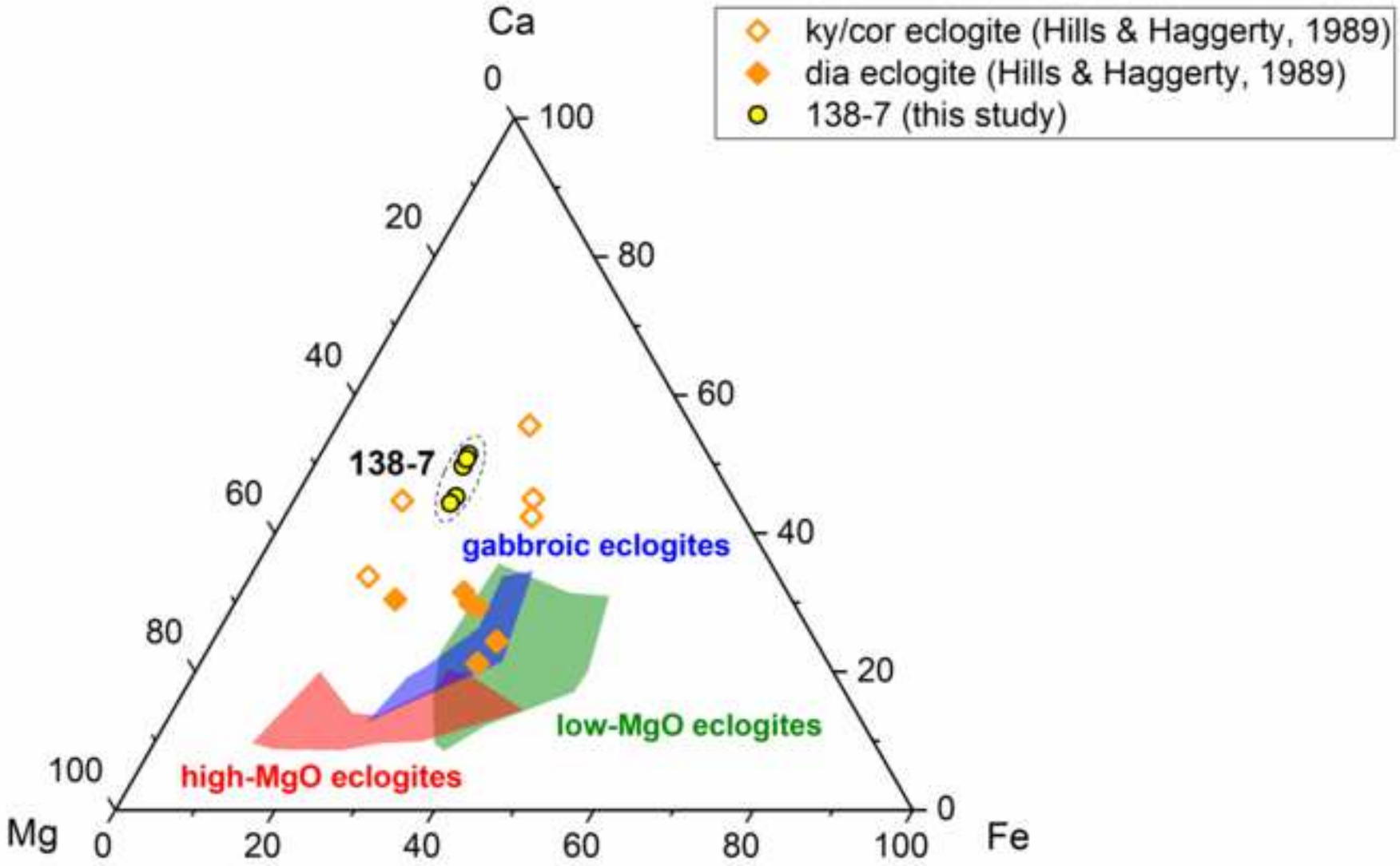

Figure 6

Click here to access/download;Figure;Figure 6_revised.tif

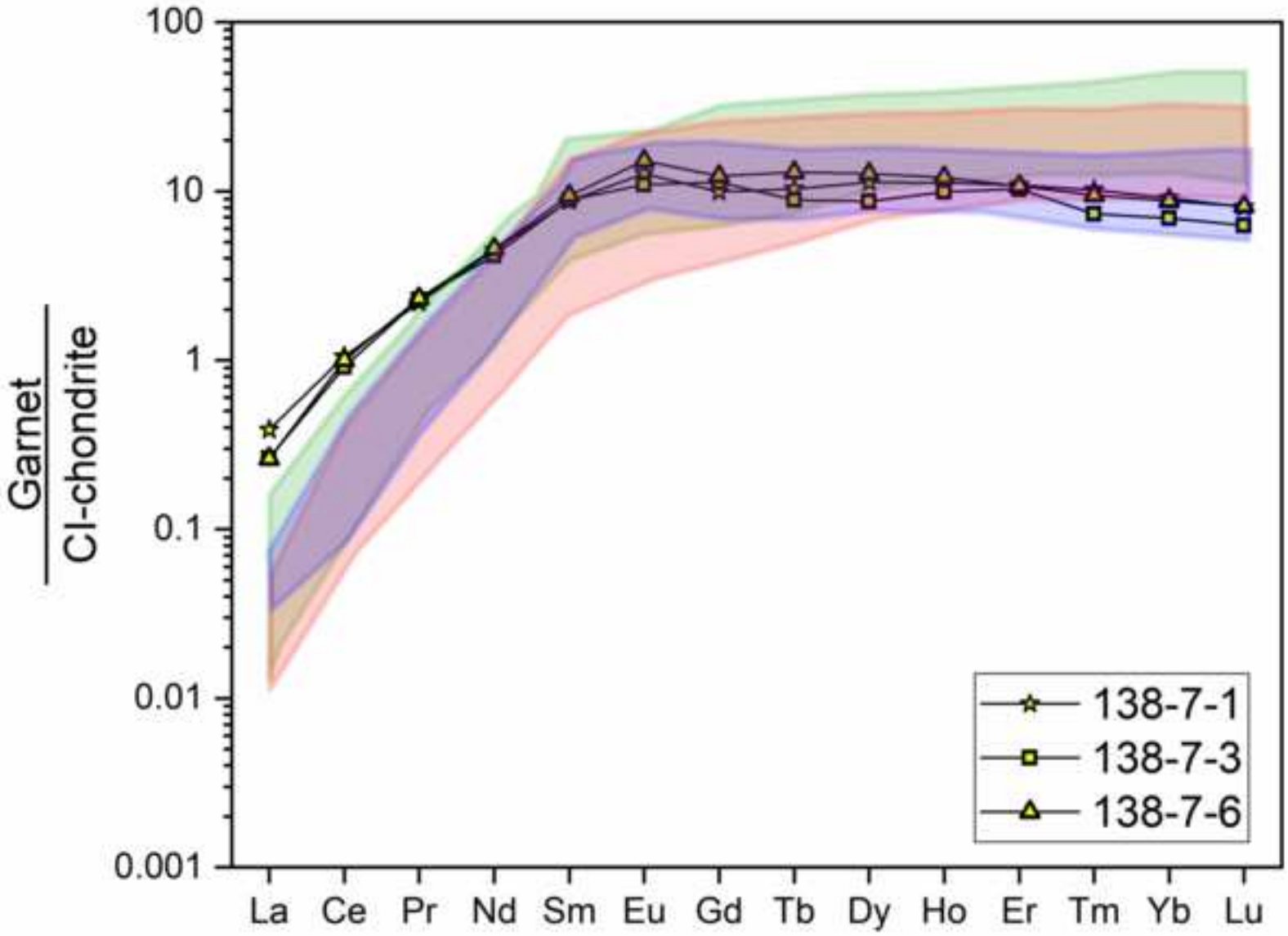

Figure 7

Click here to access/download;Figure;Figure 7_revised.tif

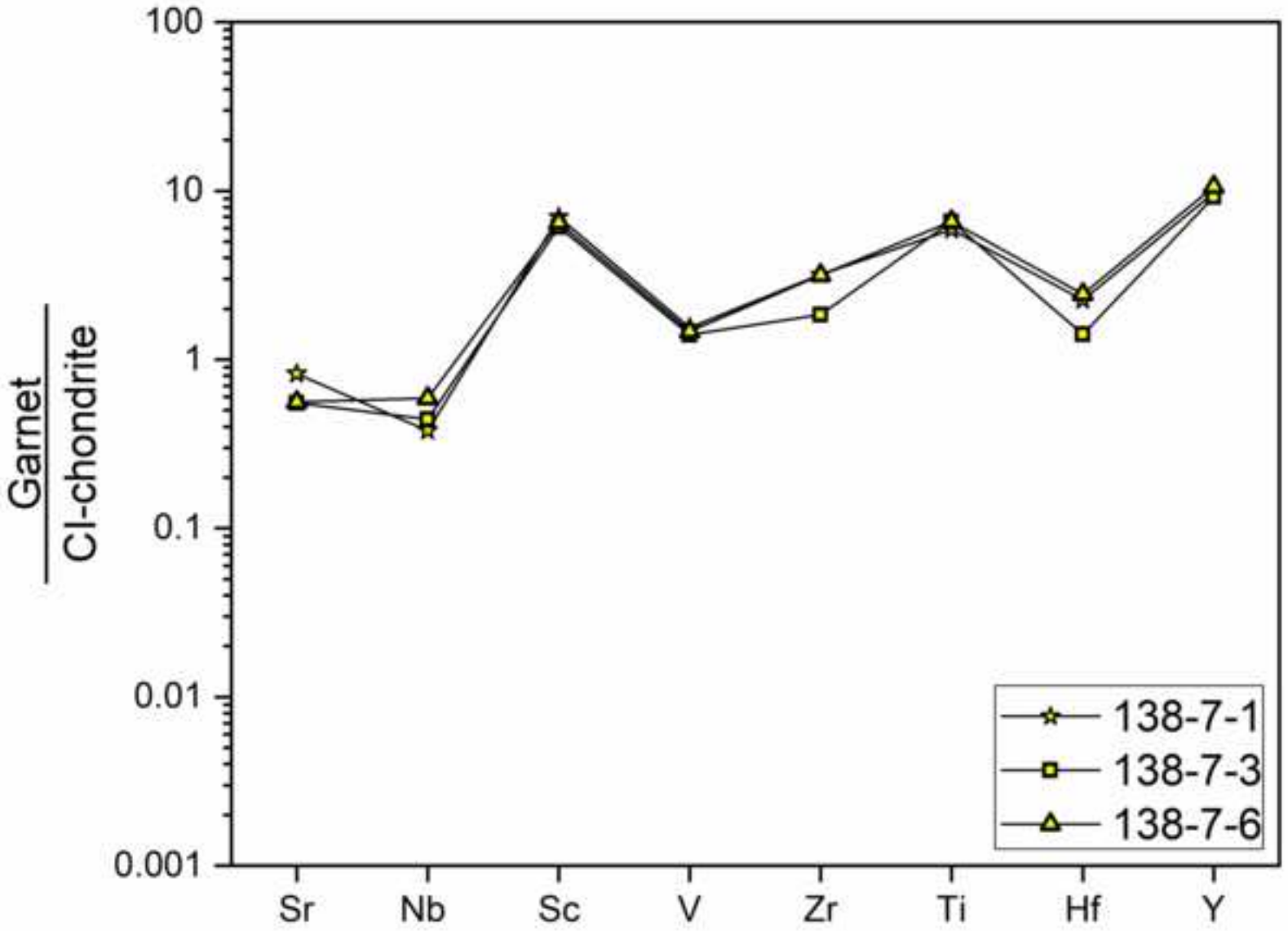

Figure 8

Click here to access/download;Figure;Figure 8.tif

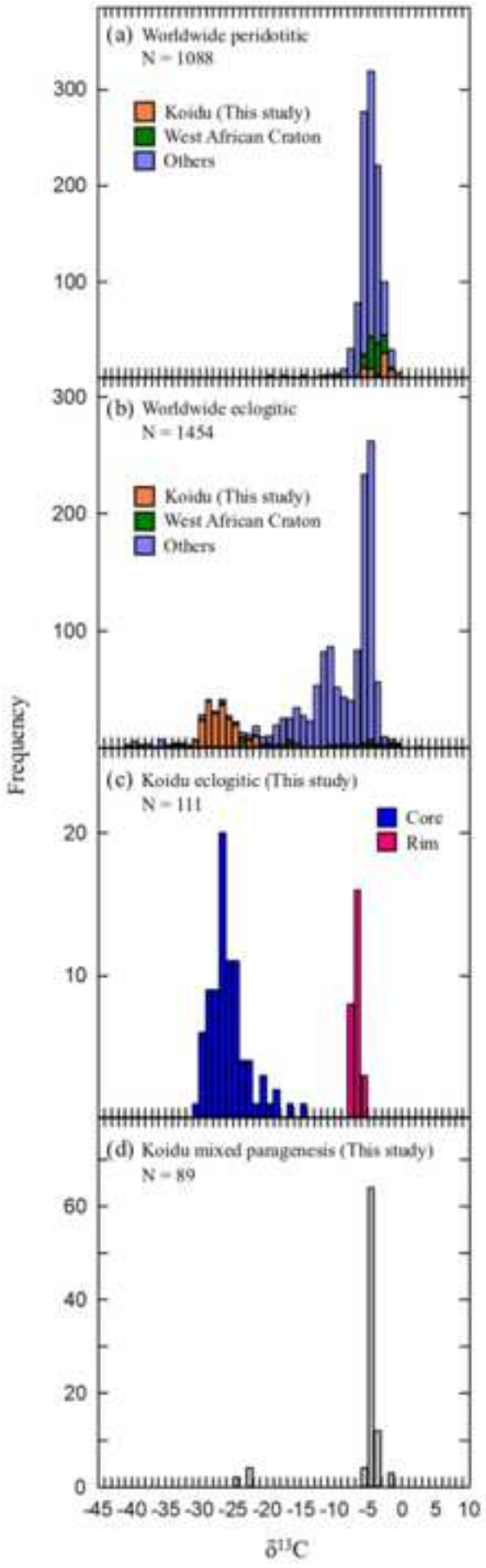

Figure 9

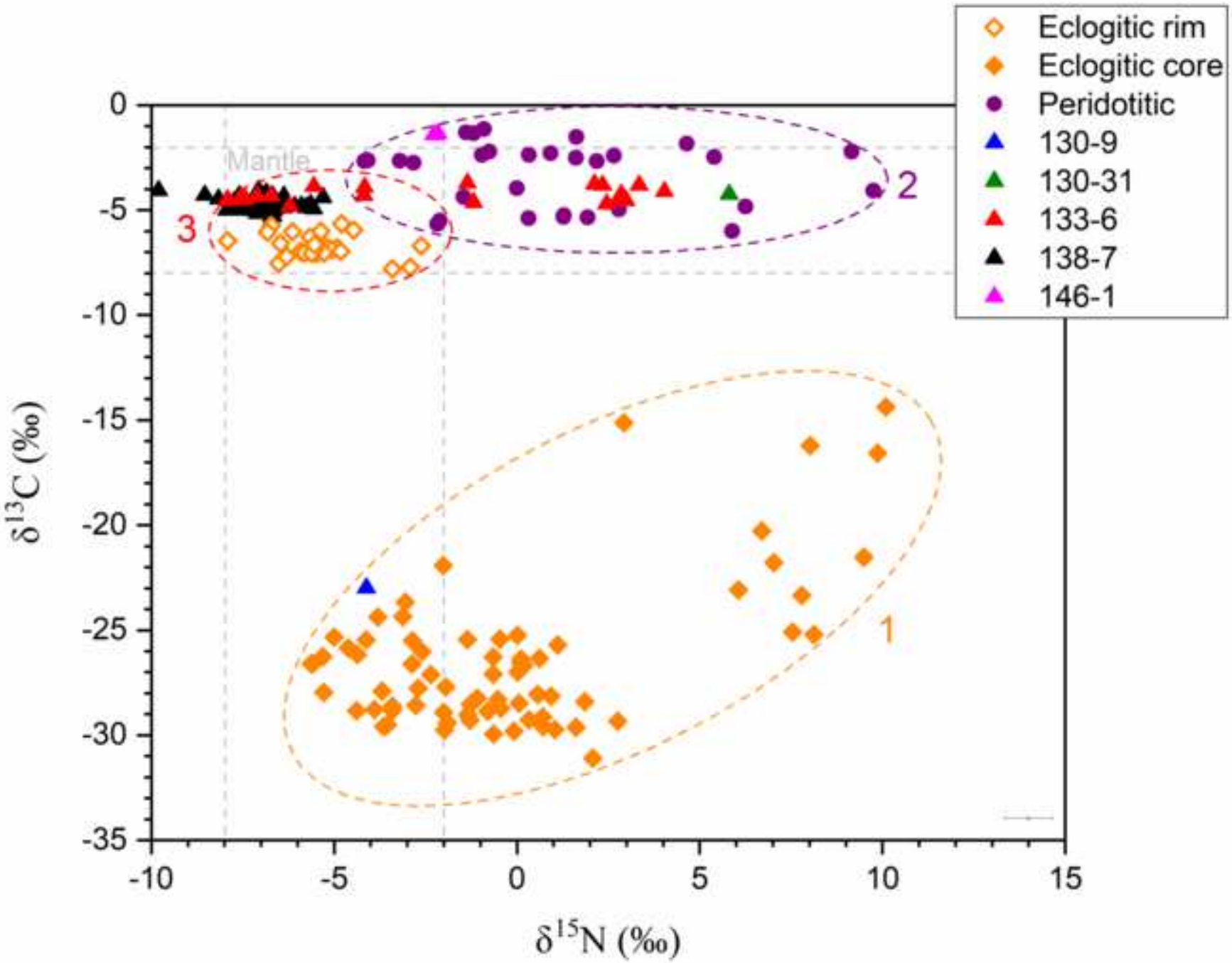

Figure 10

Click here to access/download;Figure;Figure 10.tif

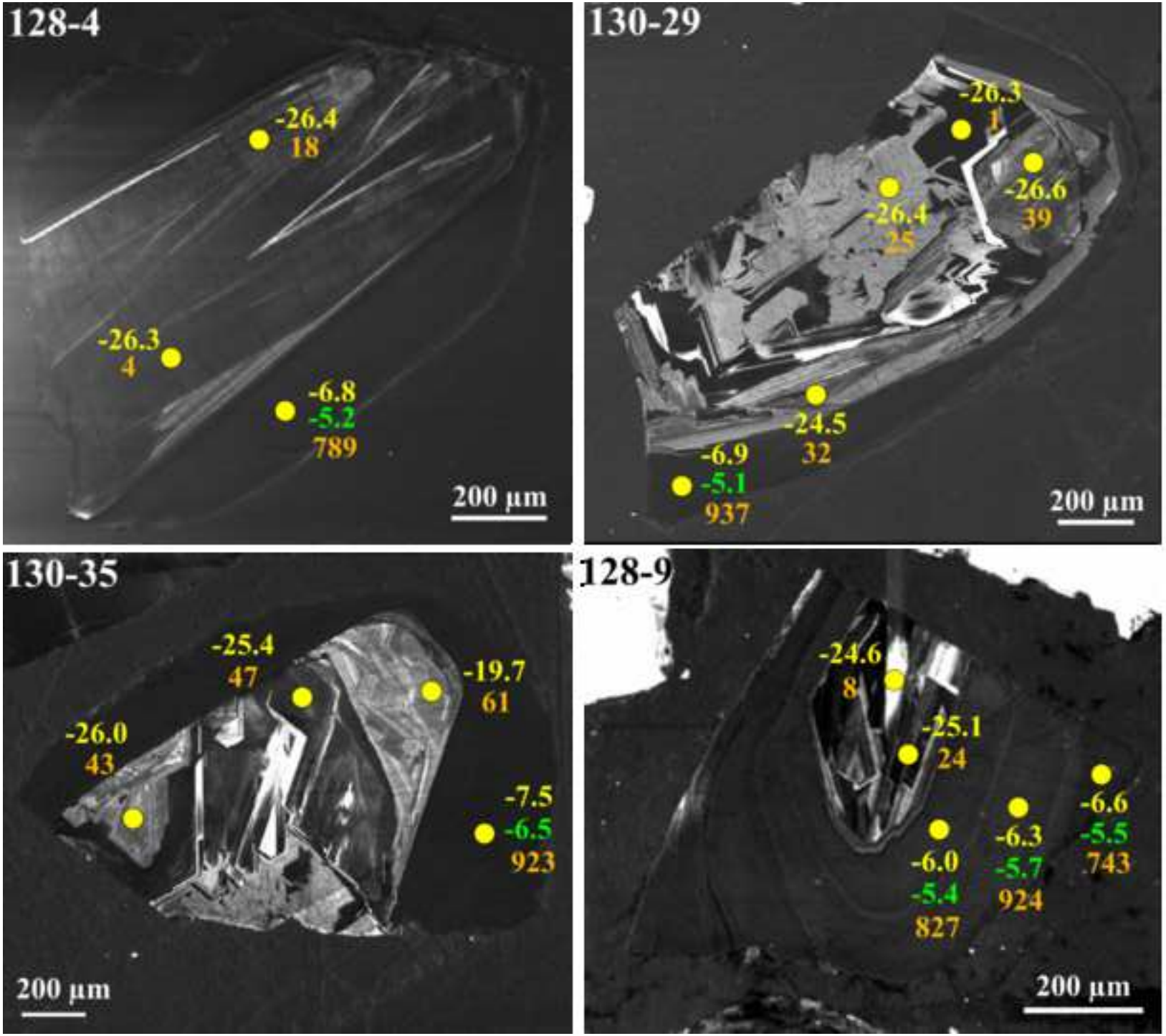

Figure 11

Click here to access/download;Figure;Figure 11_revised.png

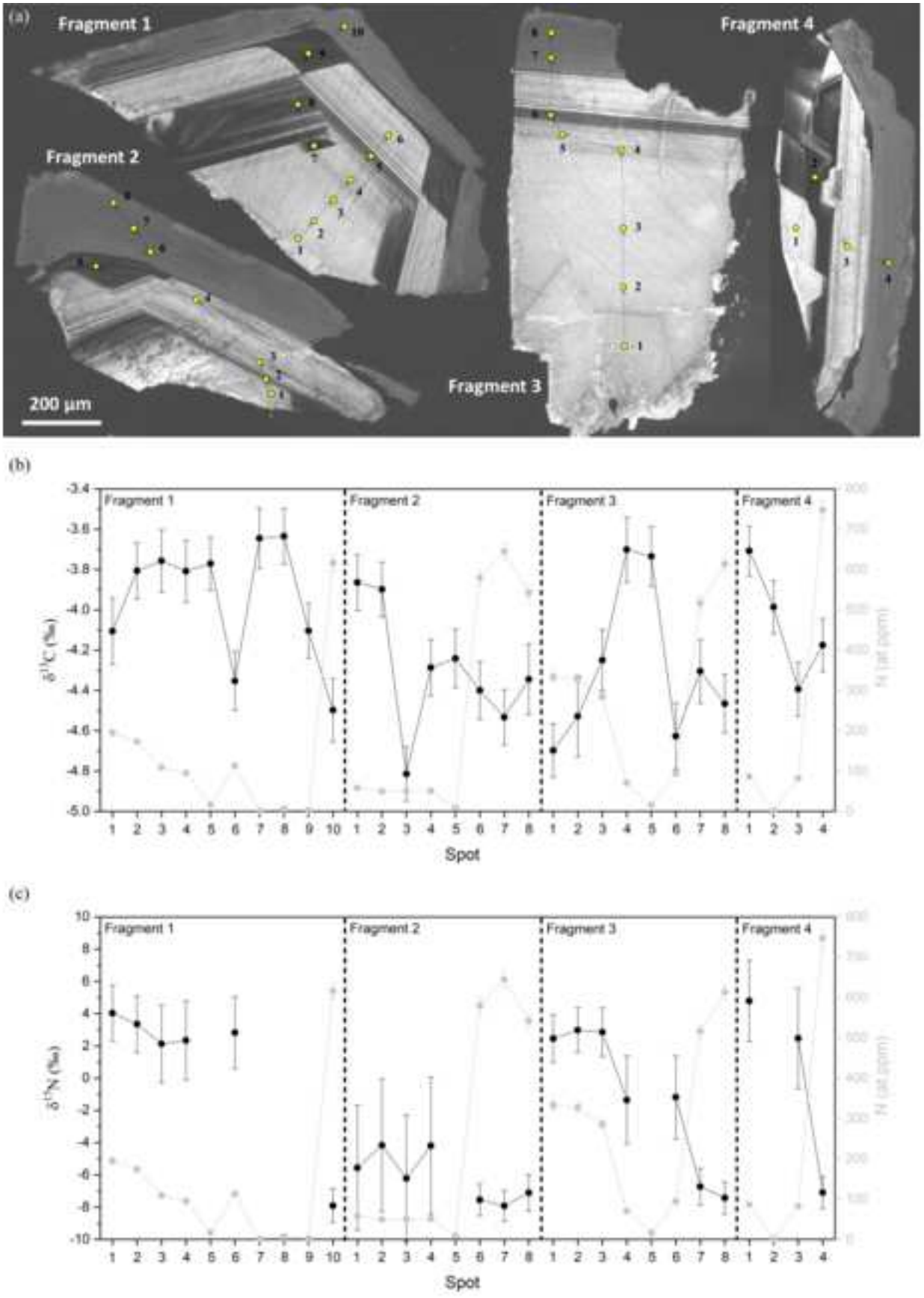

Figure 12

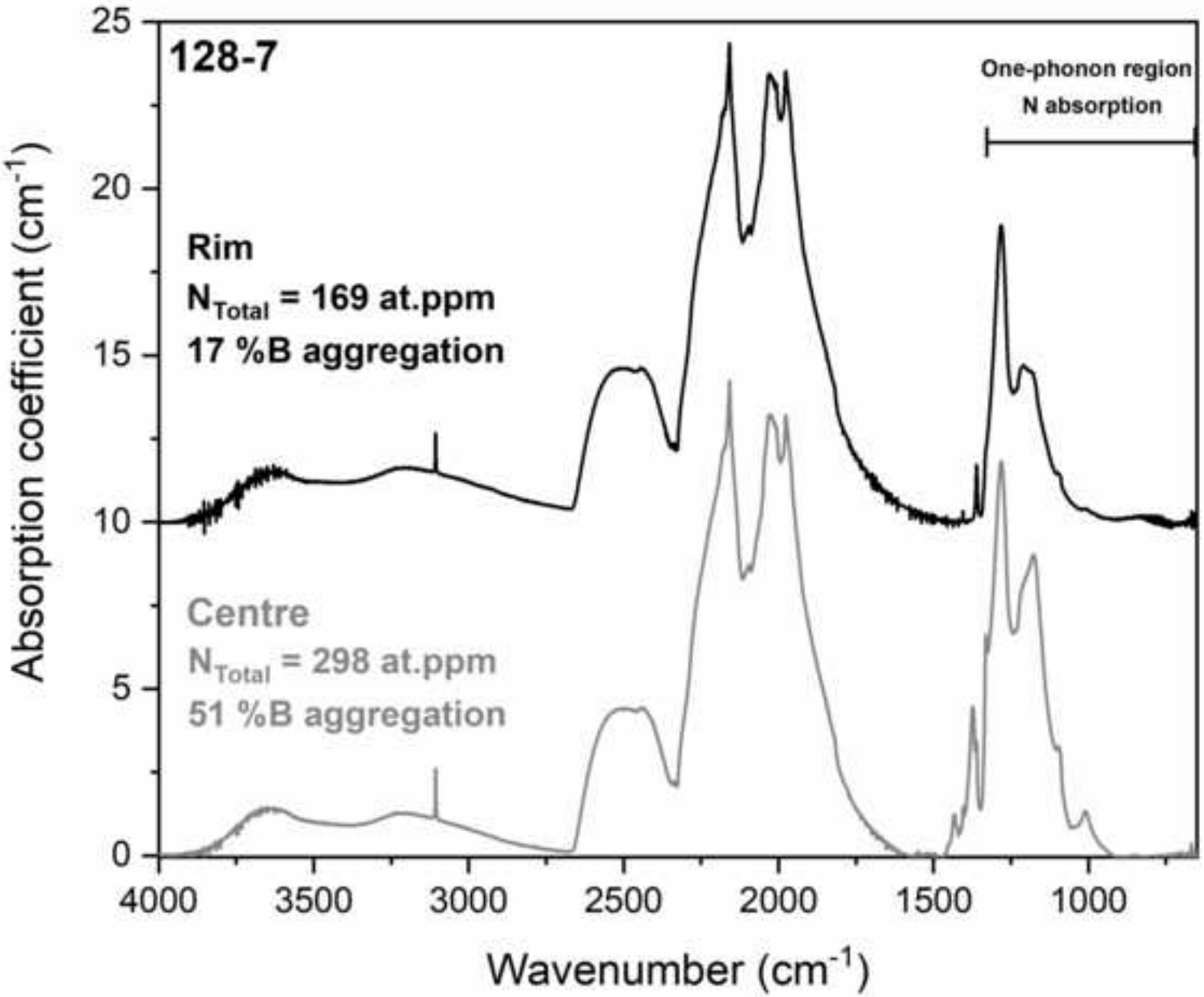

Figure 13a

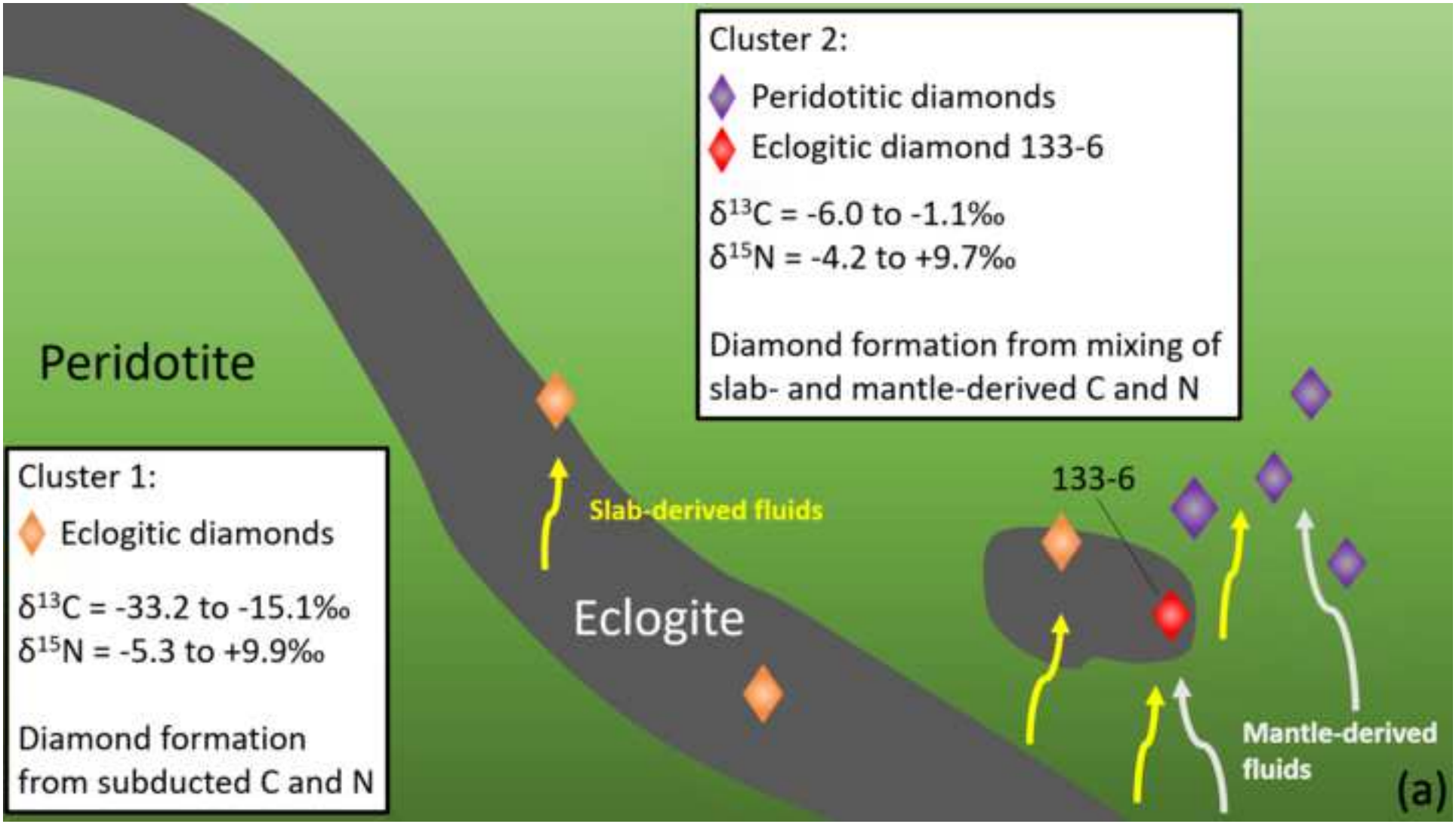

Figure 13b

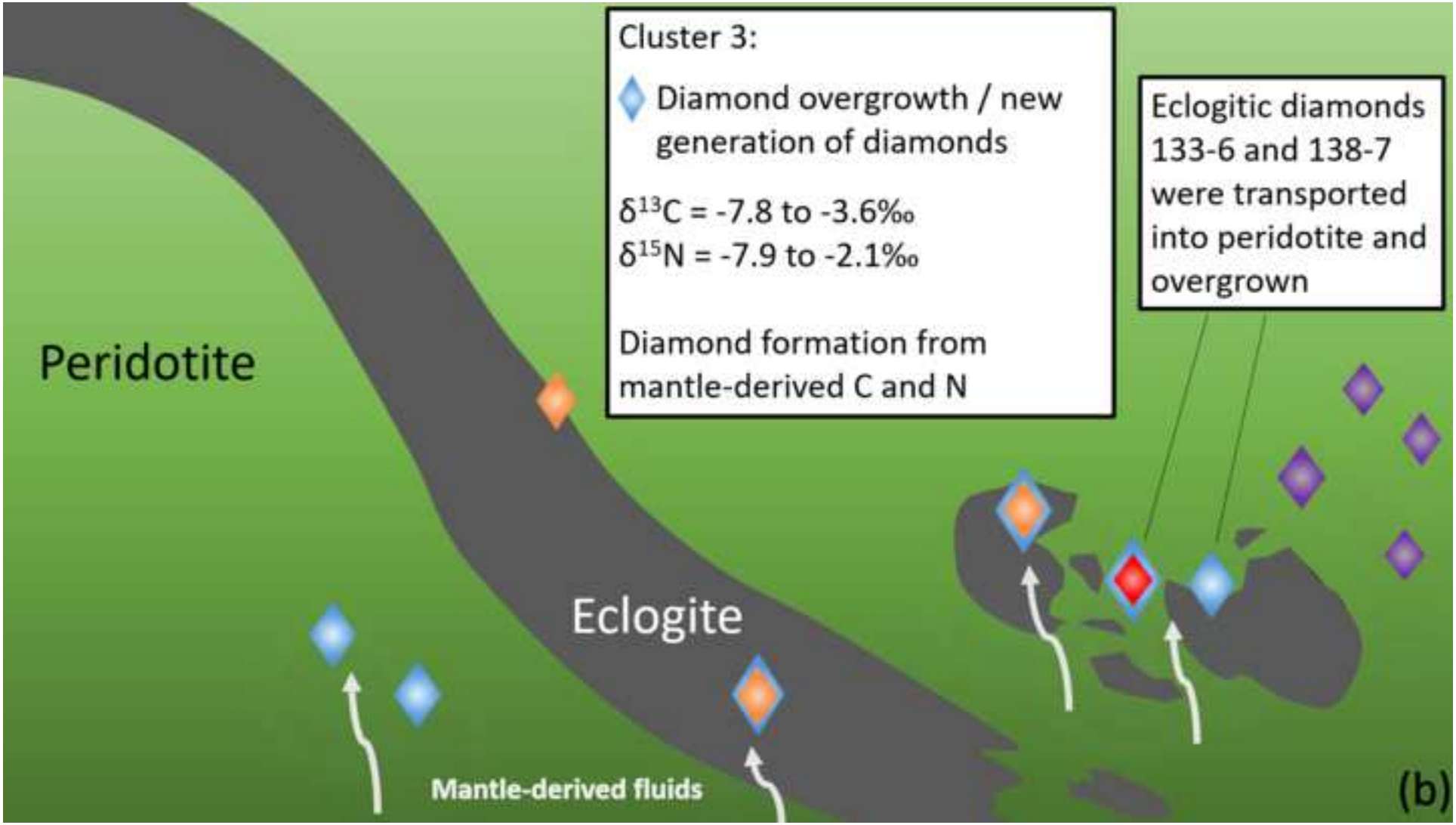

Fig. 1. Diamonds with co-occurring eclogitic and peridotitic mineral inclusions. (a) Diamond 133-6 with multiple omphacites in the centre and a Mg-chromite in the rim. (b) Diamond 138-7 with eclogitic garnets in the centre and an olivine near the rim.

Fig. 2. Ternary diagram showing the major element composition (molar Ca-Mg-Fe) of omphacite inclusions from mixed paragenesis diamond 133-6 in this study (circles). The fields for omphacites from high-MgO (red), low-MgO (green) and gabbroic eclogites (blue) (Aulbach et al., 2019c), and from kyanite- and corundum-bearing low-MgO eclogites (open diamonds) and diamond-bearing low-MgO eclogites (solid diamonds) (Hills and Haggerty, 1989) are shown for comparison. Also shown are omphacites from two low-MgO eclogites from the Obnazhennaya kimberlite in Siberia (overlapping stars; Sun et al., 2020) and from a kyanite eclogite from the Bellsbank kimberlite in South Africa (triangle; Shu et al., 2016).

Fig. 3. REE concentrations in omphacites from mixed paragenesis diamond 133-6, normalized to CI-chondrite (McDonough and Sun, 1995). These omphacites have highly fractionated (La_N/Yb_N = 422) REE_N patterns. The fields for omphacites from high-MgO (red), low-MgO (green) and gabbroic eclogites (blue) (Aulbach et al., 2019c) are shown for comparison. Also shown are the REE_N patterns of omphacites from two low-MgO eclogites from the Obnazhennaya kimberlite in Siberia (red dashed lines; Sun et al., 2020) and from a kyanite eclogite from the Bellsbank kimberlite in South Africa (magenta dotted line; Shu et al. 2016), which are very similar to our Koidu samples.

Fig. 4. Concentrations of other trace elements including LILE and HFSE in omphacites from mixed paragenesis diamond 133-6, normalized to CI-chondrite (McDonough and Sun, 1995). Also shown are the omphacites from two low-MgO eclogites from the Obnazhennaya kimberlite in Siberia (red dashed lines; Sun et al., 2020) and from a kyanite eclogite from the Bellsbank kimberlite in South Africa (magenta dotted line; Shu et al., 2016). As already seen for the REE, these omphacites have overall very similar trace element patterns to our samples. Elements are arranged in increasing compatibility in the clinopyroxene structure (Green, 1994).

Fig. 5. Ternary diagram showing the major element compositions (molar Ca-Mg-Fe) of garnet inclusions from mixed paragenesis diamond 138-7 (open circles). The fields for garnets from high-MgO (red), low-MgO (green) and gabbroic eclogites (blue) (Aulbach et al., 2019c) and from kyanite- and corundum-bearing low-MgO eclogites (open diamonds) and diamond-bearing low-MgO eclogites (solid diamonds) (Hills and Haggerty, 1989) are shown for comparison.

Fig. 6. REE concentrations in garnets from mixed paragenesis diamond 138-7, normalized to CI-chondrite (McDonough and Sun, 1995). The fields for garnets from high-MgO (red), low-MgO (green) and gabbroic eclogites (blue) (Aulbach et al., 2019c) are shown for comparison.

Fig. 7. Concentrations of other trace elements including LILE and HFSE in garnets from mixed paragenesis diamond 138-7, normalized to CI-chondrite (McDonough and Sun, 1995). Elements are arranged in increasing compatibility in the garnet structure (Green, 1994).

Fig. 8. Distribution of $\delta^{13}C$ values (individual SIMS analysis spots) in (a) peridotitic diamonds, (b) eclogitic diamonds (only diamonds without a core-rim structure are shown), (c) eclogitic diamonds with a core–rim structure and (d) mixed paragenesis diamonds in this study. Both peridotitic (a) and unzoned

eclogitic (b) Koidu diamonds are compared to diamonds from other localities on the West African Craton and from worldwide sources (database of Stachel et al., 2022).

Fig. 9. $\delta^{13}C$ versus $\delta^{15}N$ for peridotitic (circles), eclogitic (solid diamonds: core; open diamonds: rim) and mixed paragenesis diamonds (triangles) from Koidu. The error bars in the lower right corner indicated the typical total analytical uncertainties (95% confidence level). Three major compositional clusters are identified for Koidu diamonds: Cluster 1 ($\delta^{13}C$ = -33.2 to -14.4 ‰; $\delta^{15}N$ = -5.3 to +10.1 ‰), Cluster 2 ($\delta^{13}C$ = -6.0 to -1.1 ‰; $\delta^{15}N$ = -4.2 to +9.7 ‰) and Cluster 3 ($\delta^{13}C$ = -7.8 to -3.6 ‰; $\delta^{15}N$ = -7.9 to -2.1 ‰).

Fig. 10. Examples of cathodoluminescence images of Koidu eclogitic diamonds (128-4, 128-9, 130-29 and 130-35) showing core–rim structures. SIMS measurement spots with $\delta^{13}C$ values (‰; yellow), $\delta^{15}N$ values (‰; green) and N concentrations (at.ppm; orange) are indicated.

Fig. 11. (a) Cathodoluminescence images of four fragments of mixed paragenesis diamond 133-6. The yellow dots indicate the spots of SIMS analyses. (b) Core-to-rim transects across the four fragments showing variations in $\delta^{13}C$ (‰; black) and N concentration (at.ppm; grey). (c) Core to rim variations across the same fragments for $\delta^{15}N$ (‰; black) and N concentration (at.ppm; grey). The total uncertainty (95% confidence level) for each point is indicated by error bars unless they are smaller than the size of the symbol.

Fig. 12. Infrared absorption spectra of a Koidu diamond (diamond 128-7) collected through its centre (grey) and rim (black). Nitrogen absorption bands in the one-phonon region (~1332 to ~400 cm^{-1}) of the spectra show a higher degree of N aggregation (higher percentage of N in B aggregation) in the centre compared to the rim.

Fig. 13. Schematic diagram showing the growth episodes reflected by Koidu diamonds. (a) Cluster 1 diamonds (cores of eclogitic diamonds indicated by orange diamond symbol) formed from subducted crustal material (± a mantle component). Cluster 2 diamonds (core of mixed paragenesis diamond 133-6 indicated by red diamond symbol, and peridotitic diamonds indicated by purple diamond symbol) formed from mixing of slab- and mantle-derived C and N. Note that the temporal relationship between Cluster 1 and 2 is unconstrained. (b) Cluster 3 diamonds (rims of eclogitic diamonds and of mixed paragenesis diamond 133-6, mixed paragenesis diamond 138-7 and potentially some peridotitic diamonds indicated by blue diamond symbol) formed from purely mantle-derived C and N. Mixed paragenesis diamonds 133-6 and 138-7 originally formed in eclogite (encapsulating omphacites and eclogitic garnets, respectively) and were then physically transported into surrounding peridotites, where renewed diamond growth encapsulated peridotitic minerals (Mg-chromite and olivine, respectively).